The Dissertation Committee for Ethan Oblak
certifies that this is the approved version of the following dissertation:

Towards neurally guided physical therapy

Committee:

James Sulzer, Supervisor

Jarrod Lewis-Peacock, Co-Supervisor

Larry Abraham

Ashish Deshpande

Dragan Djurdjanovic

Towards neurally guided physical therapy

by

Ethan Oblak

DISSERTATION

Presented to the Faculty of the Graduate School of

The University of Texas at Austin

in Partial Fulfillment

of the Requirements

for the Degree of

DOCTOR OF PHILOSOPHY

THE UNIVERSITY OF TEXAS AT AUSTIN

December 2019

Acknowledgments

I would like to thank all those who made this work possible. My advisors, James Sulzer and Jarrod Lewis-Peacock - for introducing me to the neuroscience world, an opportunity I never imagined before joining graduate school, and for ensuring funding throughout my studies, which allowed me to delve deep into my research. My colleagues and labmates in both engineering and neuroscience - for their support and constant feedback. Remy - for always lending his eyes to new ideas. Katie and Shellie - without whose help it would have been impossible to coordinate the experiments in this dissertation. Virginia and Eli - who were instrumental in developing and testing the tasks used in this work. Finally, funding sources - this work was financially supported by a U.T. BRAIN seed grant from The University of Texas System Neuroscience and Neurotechnology Research Institute, pilot funding from the National Institutes of Health National Center of Neuromodulation for Rehabilitation (NIH/NICHD Grant Number P2CHD0886844) which was awarded to the Medical University of South Carolina, and a Robert J. Kleberg, Jr. and Helen C. Kleberg Foundation Medical Research Grant.

Towards neurally guided physical therapy

Publication No. _____

Ethan Oblak, Ph.D.
The University of Texas at Austin, 2019

Supervisors: James Sulzer
Jarrod Lewis-Peacock

Fine motor skills such as individual finger movements are impaired after neurological injury (e.g. stroke). Conventional therapy, operating at the limb, has limited success in rehabilitating fine motor skills after stroke. This work lays the foundation for guiding physical therapy of the hand from the brain, rather than from the limb. This work aims to answer three fundamental questions: **(1)** how do people learn to control their own neural activity? **(2)** how can we best decode patterns of neural activity related to individual fingers? **(3)** can people learn to shift the patterns of neural activity associated with each of their fingers?

We first investigated how people learn to control their own neural activity. Neurofeedback experiments in the MRI scanner are expensive, time-consuming, and rely on human participants to learn to control their own brain activity. Minor errors in data processing, feedback delivery, or instructions to participants can ruin an fMRI neurofeedback experiment, without any indication as to what was the problem. Here, we investigate how the properties of the fMRI

signal, feedback timing, and self-regulation strategies affect this learning, using a simulated neurofeedback environment to compare how participants' strategies interact with feedback timing. In an experiment with human participants playing a simple neurofeedback game with a simulated brain, continuous feedback led to faster learning than an intermittent feedback signal. However, in a computer model of automatic reward-based learning, intermittent feedback was more reliable. These results provide critical guidelines to the design of fMRI neurofeedback experiments.

Next, we developed techniques to most accurately decode individual finger presses in real-time from fMRI recordings. The neural correlates of individual finger movements can be revealed using multivoxel pattern analysis (MVPA) of fMRI data. Neurofeedback of MVPA, known as decoded neurofeedback, has manipulated behaviors such as visual perception and confidence judgements. However, this technique has yet to be applied to sensorimotor behaviors associated with individual fingers. Here we investigated how best to decode patterns of neural activity from sensorimotor cortex in real-time. To set key parameters for the experiment, we used offline simulations of decoded neurofeedback using previously recorded fMRI data to predict neurofeedback performance. We show that these predictions align with real neurofeedback performance at the group level and can also explain individual differences in neurofeedback success.

Finally, we investigated if people could learn to shift the neural patterns related to their own finger movements, and how this might affect fine motor skills. Deficits in individual finger movements after stroke are associated with

weakened, overlapping neural activity patterns. Here we investigated whether neural activity patterns of fingers in sensorimotor cortex could be shifted using decoded neurofeedback in healthy individuals. This is meant to provide the groundwork to using neurofeedback on stroke patients, except in the opposite direction, by decreasing confusion between finger pairs instead of increasing confusion between them. We discovered that participants could learn to shift the pattern associated with their ring finger but not that of their middle finger. We also found that participants' finger movement behaviors changed in the ring and little fingers, but not in the index or middle fingers. Our results show that neural activity and behaviors associated with the ring finger are more readily modulated than those associated with the middle finger. These results have broader implications for rehabilitation of individual finger movements, which may be limited or enhanced by individual finger plasticity after neurological injury.

Table of Contents

List of Tables

List of Figures

Chapter 1

Introduction[1]

1.1 Neurofeedback: background and learning mechanisms

Neuroimaging studies often find correlations between behaviors and recorded neural activation. To test whether these relationships are causal, neuroscientists must find a way to manipulate the underlying neural structure and observe whether the associated behavior is affected. In human neuroscience research, we are usually limited to noninvasive methods that have minimal associated risk. Currently, safe and noninvasive neural stimulation techniques such as transcranial magnetic stimulation (TMS) and transcranial direct-current stimulation (tDCS) can only affect neural structures on the scale of centimeters [75, 9]. These techniques are too coarse to manipulate behaviors that correlate with the millimeter-scale patterns of neural activation recorded by functional magnetic resonance imaging (fMRI). Using multi-voxel pattern analysis (MVPA [52]),

[1] Portions of this chapter were published in the following two articles: “Self-regulation strategy, feedback timing and hemodynamic properties modulate learning in a simulated fMRI neurofeedback environment" published in PLOS Computational Biology 2017. Oblak, Ethan F.; Lewis-Peacock, Jarrod A.; Sulzer, James S., Public Library of Science, 2017. “A simulation-based approach to improve decoded neurofeedback performance" published in NeuroImage 2019. Oblak, Ethan F.; Sulzer, James S.; Lewis-Peacock, Jarrod A., Elsevier, 2019. The dissertation author was the primary author of both manuscripts. For the content contained in this chapter, the author carried out a literature review of neurofeedback and fMRI pattern decoding, including learning mechanisms and applications to sensorimotor cortex.

we can identify neural features such as orientation tuning [38, 33] and complex motor programs [79, 44] which are inaccessible to other human neuroimaging analysis methods.

Although we cannot exogenously stimulate these patterns, it is possible for people to endogenously activate them if they are presented with visual feedback of the recorded activity pattern in a procedure known as fMRI neurofeedback [65]. In this procedure, people must learn to elicit a targeted neural activation pattern by observing a feedback signal and adjusting their strategy to maximize this signal (Fig 1.1A). This technique faces challenges as many participants are unable to self-regulate. This “non-responder effect" has been quantified in electroencephalography (EEG) neurofeedback, with 15-30% of neurofeedback participants being completely unable to self-regulate [2, 28]. EEG researchers have correlated this effect with resting-state activity [5], white matter tract integrity [27], technological knowledge [82], and sense of agency [22].

For fMRI neurofeedback, the causes of the non-responder effect have not been identified due to the cost and complexity of examining all possible factors in the MRI scanner. We believe that the characteristics of the signal measured by fMRI are critical to understanding how people learn to self-regulate. Instead of directly measuring neural activity, fMRI measures a proxy signal of neural activity known as the hemodynamic response. This signal measures a contrast of oxygenated versus deoxygenated blood in small parcels (or voxels) of the brain. These voxels can vary in size, but are typically on the scale of 2-3mm, and an fMRI scan can record voxels across the entire brain within 2

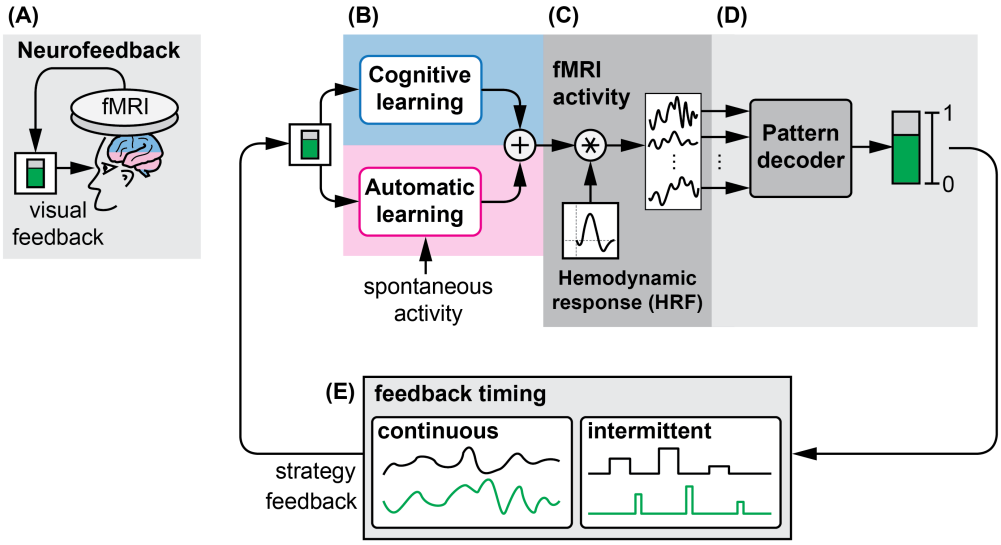

Figure 1.1: **Overview of neurofeedback. (A)** In fMRI neurofeedback, neural activity is most commonly represented as a visual thermometer, which participants attempt to raise as high as possible. **(B)** To raise the thermometer, participants can engage in cognitive strategies such as mental imagery, or they can rely on automatic learning circuits within the brain to recognize spontaneous activity that causes the thermometer to increase in size. **(C)** Activity recoded by the MRI scanner is a blurred and delayed version of underlying neural activity that has been filtered by the hemodynamic response function (HRF). **(D)** Activity throughout the brain is processed by a pattern decoder and sythesized into a single number representing how closely the current neural activity matches the desired activity pattern. **(E)** Although feedback can be delivered continuously in real-time, it is often delivered intermittently because the HRF can make it difficult to relate a continuous strategy to the delayed and blurred hemodynamic response.

seconds. This flow of oxygenated blood is a response to underlying neural activity, and is typically characterized by a 6-sec delay. However, the hemodynamic response is more precisely characterized using the canonical hemodynamic response function (HRF), which is a combination of a delay and blurring in time

relative to underlying neural activation [7, 26] (Fig 1.1C). This complex response function forms a difficult credit-assignment problem, in which participants must remember which previous behavior or underlying neural activity caused the delayed and blurred feedback to change in order to learn to self-regulate. When people explore different cognitive strategies in an attempt to control the neurofeedback signal, they must remember a time history of behaviors and determine which behavior was responsible for influencing the feedback signal (Fig 1.1B, top). To “remember" past neural activity, automatic learning circuits must hold spontaneous activity in memory [60] and reinforce it using an internal learning rule that is not cognitively accessible to the participant (Fig 1.1B, bottom). This forms a traditional reinforcement learning problem, but in which the reinforcement teaching signal lags the behavior to be learned by several seconds.

The difficulty of this credit-assignment task could be reduced by appropriately scheduling feedback to account for the hemodynamic signal properties. One of the controversies in fMRI neurofeedback is whether to schedule feedback continuously or intermittently (Fig 1.1E), trading off feedback frequency to account for the hemodynamic response [67]. Only two small pilot studies have been published to address this controversy. The first study compared continuous to intermittent presentation of fMRI neurofeedback of regional activation levels from the supplementary motor area, finding that intermittent feedback produced better learning [37]. The second study found mixed results in auditory cortex, with continuous feedback showing better performance over multiple sessions [21]. Therefore, prior to our work here [53], the question of feedback

timing remained largely unanswered within the field of fMRI neurofeedback, with critical implications for neurofeedback performance.

1.2 Multi-voxel pattern analysis (MVPA)

Whereas conventional fMRI analysis looks at the average level of neural activity in different brain regions, multi-voxel pattern analysis (MVPA) extracts information about a person's cognitive state by analyzing spatially distributed patterns of functional MRI activity [49, 30]. This approach has become ubiquitous in cognitive neuroscience since the seminal work of Haxby et al. (2001) [31] identified distributed and overlapping representations of visual object categories in temporal cortex. MVPA works by identifying the tuning of each voxel to a set of different stimuli (Fig 1.2A). By training a pattern decoder on a set of data in which participants are exposed to various stimuli, new data can be decoded to obtain the likelihood that a particular stimulus was being observed at that time (Fig 1.2B).

1.3 MVPA in sensorimotor cortex: individual fingers, motor learning, and stroke recovery

Although first applied to visual perception, MVPA has more recently been applied to sensorimotor cortex. Initially, individual fingers were mapped in primary motor (M1) and somatosensory (S1) cortex of the contralateral ('controlling') hemisphere [80]. Soon after, similar pattern representations were found in the opposite, ipsilateral M1 and S1 [18]. Next, learned sequences of but-

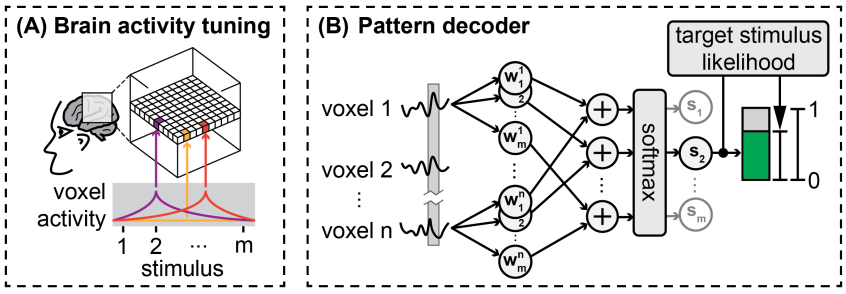

Figure 1.2: **Overview of multi-voxel pattern analysis. (A)** Each 2-3mm cube of brain activity, or voxel, recorded by fMRI responds differently to a set of stimuli. For example, given *m* different stimuli, some voxels respond strongly to certain stimulus (e.g. the purple voxel responds strongly to stimulus #2), while some voxels are unresponsive (e.g. the yellow voxel does not respond strongly to any of the *m* stimuli). **(B)** Recorded neural activity can be decoded by training a pattern decoder on brain data gathered while the participant was exposed to a set of *m* stimuli. The trained decoder will have a weight *w* for each of the *m* stimulus classes and for each of the *n* voxels recorded from the brain. By multiplying a new recorded pattern of brain activity in each voxel by the weight for all classes, and summing the combination of weighted brain activity within each class, a score is obtained for each class. The vector of *m* scores are then submitted to $softmax(\cdot) = e^{(\cdot)}/\Sigma e^{(\cdot)}$, which converts the raw scores to a set of likelihoods for each class which each lie between 0 and 1 and sum to 1. If we wish to convert the vector of decoder outputs to a single score, we can extract the likelihood for a single stimulus class (in this example, we chose the likelihood for stimulus #2).

ton presses were mapped not only in M1 and S1, but also premotor cortex (PMC) and supplementary motor area (SMA) [79], aligning with theory and experiments from non-human primate models [51, 34]. Critically, these neural activity patterns were found to strengthen with learning of the sequence.

Further work aimed to analyze the information contained within these patterns, rather than simply seeing which brain areas were sufficient to decode

between different digits or sequences. Mirrored sequences performed with opposite hands were found to have overlapping representations in M1 and S1, whereas visually identical sequences performed with opposite hands showed overlapping representations in PMC and SMA [81]. Timing of sequences was also shown to overlap in PMC, again aligning with predictions from animal models [44]. While sequences appear to be well-defined using MVPA, one critical issue was recently discovered: sequence representations are highly overlapping with individual digit representations [87]. Specifically, the neural activity pattern for a sequence was heavily biased toward the first finger of the sequence, which is hypothesized to be due to motor preparatory neural activity before the first press.

The representation of individual fingers in primary somatosensory cortex is therefore a more robust decoding target, with recent studies showing a rich representational structure across sensorimotor cortex that aligns with natural hand use [19]. Furthermore, these patterns can degrade after stroke [84] and can even be altered by temporarily impairing healthy participants [42], in this case by gluing two of the fingers together for 24 hours. These individual finger representations are therefore a potential target for neurotherapeutic intervention such as neural stimulation or neurofeedback.

1.4 Decoded neurofeedback

Investigation into causal mechanisms of MVPA representations of neural activity requires this activity to be modulated. As mentioned earlier, current

top-of-the-line neural stimulation techniques such as TMS [75] and tDCS [9] are incapable of modulating fine-grained patterns of neural activity. Operant conditioning of neural activity, known as neurofeedback, uniquely enables self-modulation of a target neural circuit through feedback, most often presented visually [67, 65]. Early work in fMRI neurofeedback mirrored contemporary univariate techniques in offline fMRI analysis, in which the average neural activity in a region is modulated [58]. In recent years, MVPA-based neurofeedback techniques have taken hold [47]. For instance, a seminal work by Shibata et al. (2011) [64] used neurofeedback based on decoded activity from early visual cortex, a process dubbed 'decoded neurofeedback' or 'DecNef'. The researchers were able to show that individuals could learn to self-modulate a targeted pattern of brain activity related to a given orientation of a visual grating without stimulus presentation. Intriguingly this was associated with heightened perceptual acuity specific to the underlying stimulus. Thus, used in this manner, decoded neurofeedback is a powerful and unique tool in neuroscience that can manipulate neural activity patterns to reveal causal relationships with behavior. This technique has been used in several applications beyond low-level visual perception, including fear conditioning [41], confidence judgements [12], and facial preference [63]. To date, this technique has not yet been applied to sensorimotor cortex, but could provide a method to investigate motor behavior and stroke recovery if used on MVPA representations of individual fingers or sequences of finger presses.

1.5 Application of decoded neurofeedback to sensorimotor cortex

The work in this dissertation is the first application of decoded neurofeedback to motor skills and sensorimotor cortex. When we initally attempted to perform decoded neurofeedback experiments, we found that participants were unable to learn to control their own neural activity. Therefore, we needed to create the groundwork for decoded neurofeedback in sensorimotor cortex by first creating a comprehensive simulation of neurofeedback to understand how participants learn to control their own neural signals, and then apply this simulation to sensorimotor cortex and perform a real neurofeedback experiment to validate these results. After overcoming these hurdles, and revealing several principles of neural self-regulation along the way, we are able to perform a decoded neurofeedback experiment targeting fine motor skills and sensory behavior related to individual fingers.

Chapter 2

Simulated neurofeedback reveals principles of neural self-regulation[1]

Abstract

Direct manipulation of brain activity can be used to investigate causal brain-behavior relationships. Current noninvasive neural stimulation techniques are too coarse to manipulate behaviors that correlate with fine-grained spatial patterns recorded by fMRI. However, these activity patterns can be manipulated by having people learn to self-regulate their own recorded neural activity. This technique, known as fMRI neurofeedback, faces challenges as many participants are unable to self-regulate. The causes of this non-responder effect are not well understood due to the cost and complexity of such investigation in the MRI scanner. Here, we investigated the temporal dynamics of the hemodynamic response measured by fMRI as a potential cause of the non-responder effect. Learning to self-regulate the hemodynamic response involves a difficult temporal credit-assignment problem because this signal is both delayed and

[1]This chapter, in full, was published as an article entitled “Self-regulation strategy, feedback timing and hemodynamic properties modulate learning in a simulated fMRI neurofeedback environment" published in PLOS Computational Biology 2017. Oblak, Ethan F.; Lewis-Peacock, Jarrod A.; Sulzer, James S., Public Library of Science, 2017. The dissertation author was the primary author of the manuscript. The author was responsible for conceptualization and design of the experiment, as well as analysis and visualization of this research.

blurred over time. Two factors critical to this problem are the prescribed self-regulation strategy (cognitive or automatic) and feedback timing (continuous or intermittent). Here, we sought to evaluate how these factors interact with the temporal dynamics of fMRI without using the MRI scanner. We first examined the role of cognitive strategies by having participants learn to regulate a simulated neurofeedback signal using a unidimensional strategy: pressing one of two buttons to rotate a visual grating that stimulates a model of visual cortex. Under these conditions, continuous feedback led to faster regulation compared to intermittent feedback. Yet, since many neurofeedback studies prescribe implicit self-regulation strategies, we created a computational model of automatic reward-based learning to examine whether this result held true for automatic processing. When feedback was delayed and blurred based on the hemodynamics of fMRI, this model learned more reliably from intermittent feedback compared to continuous feedback. These results suggest that different self-regulation mechanisms prefer different feedback timings, and that these factors can be effectively explored and optimized via simulation prior to deployment in the MRI scanner.

2.1 Introduction

Neuroimaging studies often find correlations between behaviors and recorded neural activation. To test whether these relationships are causal, neuroscientists must find a way to manipulate the underlying neural structure and observe whether the associated behavior is affected. In human neuroscience research,

we are usually limited to noninvasive methods that have minimal associated risk. Currently, safe and noninvasive neural stimulation techniques such as transcranial magnetic stimulation (TMS) and transcranial direct-current stimulation (tDCS) can only affect neural structures on the scale of centimeters [75, 9]. These techniques are too coarse to manipulate behaviors that correlate with the millimeter-scale patterns of neural activation recorded by functional magnetic resonance imaging (fMRI). Using multi-voxel pattern analysis (MVPA [52]), we can identify neural features such as orientation tuning [38, 33] and complex motor programs [79, 44] which are inaccessible to other human neuroimaging analysis methods.

Although we cannot exogenously stimulate these patterns, it is possible for people to endogenously activate them if they are presented with visual feedback of the recorded activity pattern in a procedure known as fMRI neurofeedback [66]. In this procedure, people must learn to elicit a targeted neural activation pattern by observing a feedback signal and adjusting their strategy to maximize this signal (Fig 2.1A). This technique faces challenges as many participants are unable to self-regulate. This “non-responder effect" has been quantified in electroencephalography (EEG) neurofeedback, with 15-30% of neurofeedback participants being completely unable to self-regulate [2, 28]. EEG researchers have correlated this effect with resting-state activity [5], white matter tract integrity [27], technological knowledge [82], and sense of agency [22].

For fMRI neurofeedback, the causes of the non-responder effect have not been identified due to the cost and complexity of examining all possible

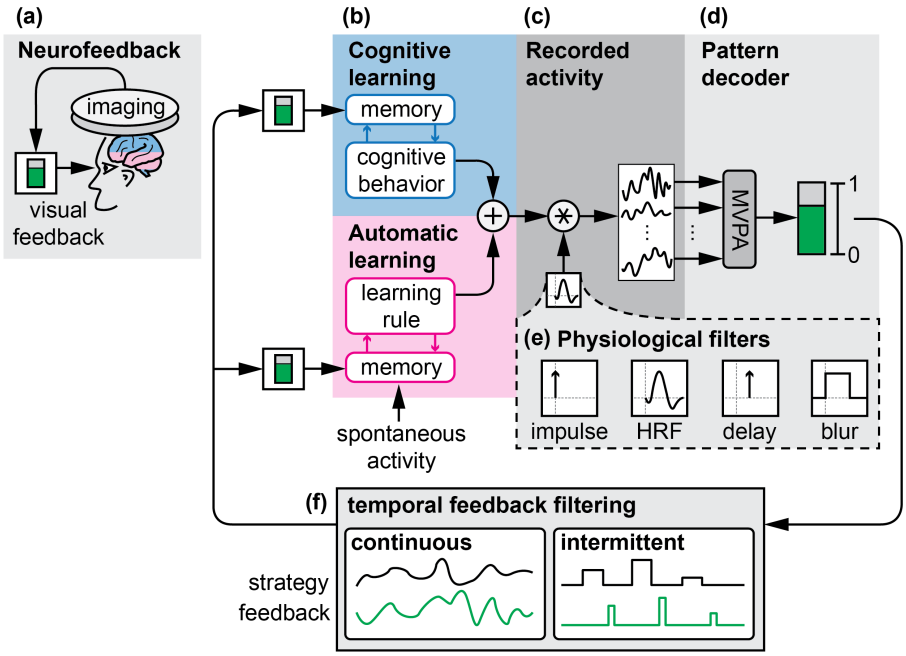

Figure 2.1: **System model of neurofeedback. (A)** Neurofeedback is biofeedback of neural activity, commonly presented as a visual thermometer (in green) that participants learn to control. **(B)** Neurofeedback is learned through either cognitive or automatic learning processes. In cognitive learning, participants try various cognitive behaviors and, through trial-and-error, must learn which behaviors result in successful regulation of the feedback signal. In automatic learning, spontaneous neural activity is held in memory, and the feedback signal reinforces this neural activity according to an internal learning rule. **(C)** Underlying neural activity is convolved with a physiological filter such as the hemodynamic response function (HRF) before being recorded by neuroimaging. **(D)** A multivariate pattern analysis (MVPA) classifier is used to convert multiple channels (or voxels) of neural activity into a single value that represents how closely the recorded neural activity matches a desired pattern. **(E)** We present four candidate physiological filters: an instantaneous impulse, the canonical HRF, a 6-second delay, and a 10-second moving average blur. **(F)** Once decoded, feedback can either be presented continuously or intermittently.

factors in the MRI scanner. We believe that the characteristics of the hemodynamic response measured by fMRI are critical to understanding how people learn to self-regulate because the hemodynamic response is both delayed and blurred in time relative to underlying neural activation [7, 26]. This forms a difficult credit-assignment problem, in which participants must remember which previous behavior or underlying neural activity caused the delayed and blurred feedback to change in order to learn to self-regulate. When people explore different cognitive strategies in an attempt to control the neurofeedback signal, they must remember a time history of behaviors and determine which behavior was responsible for influencing the feedback signal (Fig 2.1B, top). To “remember" past neural activity, automatic learning circuits must hold spontaneous activity in memory [60] and reinforce it using an internal learning rule that is not cognitively accessible to the participant (Fig 2.1B, bottom).

The difficulty of this credit-assignment task could be reduced by appropriately scheduling feedback to account for the hemodynamic signal properties. One of the controversies in fMRI neurofeedback is whether to schedule feedback continuously or intermittently (Fig 2.1F), trading off feedback frequency to account for the hemodynamic response [67]. Only two small pilot studies have been published to address this controversy. The first study compared continuous to intermittent presentation of fMRI neurofeedback of regional activation levels from the supplementary motor area, finding that intermittent feedback produced better learning [37]. The second study found mixed results in auditory cortex, with continuous feedback showing better performance over multiple

sessions [21]. It is difficult to generalize these results because success may depend on other factors such as neurofeedback signal quality and self-regulation strategy. An exhaustive search of parameters within the MRI scanner is impractical due to cost. Therefore, our main goal here was to bridge the gap in understanding neurofeedback learning by testing key factors (feedback timing and self-regulation strategy) in a simulation environment outside of the MRI scanner.

We constructed a model of early visual cortex (V1) to use as a simulated neurofeedback testbed (Fig 2.2A). We chose V1 as our model because this is one of the most well-studied cortical areas, starting with early electrophysiological studies in animals [36] and extending to modern fMRI studies [74]. We specifically modeled the response of V1 to grating orientations because this has been extensively studied with fMRI [38, 33, 1]. To deliver feedback from this model, we constructed similar MVPA classifiers (Fig 2.2B) to decode grating-associated patterns during explicit presentation of stimuli [86] as well as in the absence of stimuli [64].

To model the temporal properties of the hemodynamic response, we created four different physiological filters to apply to our simulated neural signal (Fig 2.1E). The first is an impulse response, which corresponds to no delaying or blurring of the recorded signal, as if we could directly record electrophysiological activity at the spatial resolution of fMRI. Next, we simulated the fMRI blood-oxygen-level-dependent (BOLD) response, using the canonical hemodynamic response function (HRF) [7] to blur and delay the underlying neural activity. The

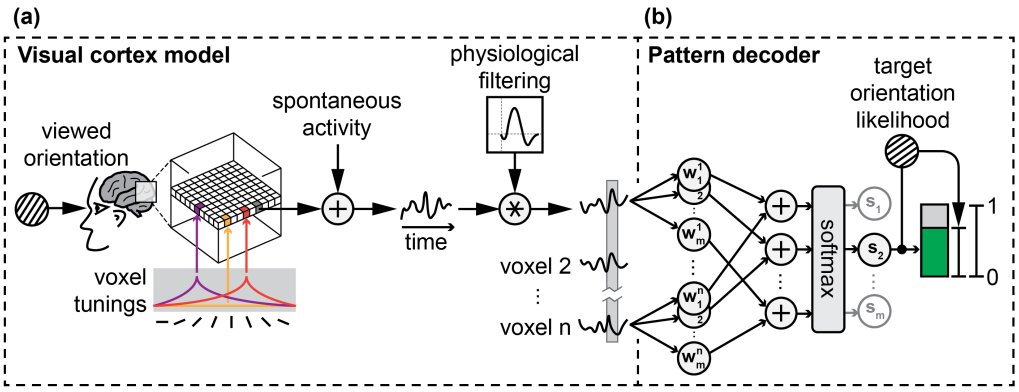

Figure 2.2: **Simulated visual cortex as measured by fMRI and decoded using MVPA. (A)** Voxels (n=1000) in the model are either tuned to one of eight orientations (0°, 22.5°, ..., 157.5°; 2.5% of voxels each), or have no orientation selectivity (80% of all voxels). All voxels have additive spontaneous activity and are convolved in time with a physiological filter such as the canonical HRF (for all candidate filters, see Fig 2.1e). **(B)** The pattern decoder transforms the measured pattern of simulated activity into a number indicating the likelihood that the activity matches the pattern associated with one of m target grating orientations. For cognitive experiments, m=8 (0°, 22.5°, ..., 157.5°); for automatic experiments, m=3 (10°, 70°, 130°).

final two filters were a 6-second delay and a 10-second moving average blur, corresponding to the delay-to-peak of the HRF and a boxcar function centered around this peak, respectively. We used these two synthetic filters to investigate the unique contribution of delay and blur to the learning of fMRI neurofeedback signals. We hypothesized that isolated delay and blur responses would be more difficult to learn than an impulse response, and that the combined delay and blur of the HRF would be the most difficult.

Using our model of V1 and the four candidate physiological filters, we first examined cognitive strategies as these are the most common type of strategy

given in traditional fMRI neurofeedback experiments [67, 66]. These strategies commonly take the form of mental imagery [17], which is notoriously difficult to quantify and relies on participants to self-report their strategy. To avoid this difficulty, we used a motor strategy as a proxy for mental imagery. Participants pressed one of two buttons to rotate a grating image that stimulated our V1 model. Participants had to discover a target orientation using a neurofeedback signal from our model that was filtered by one of the physiological filters. This allowed us to examine how people make cognitive decisions when faced with delayed or blurred feedback.

Next, we used the same model and filters to examine an alternative approach to fMRI neurofeedback: relying entirely on automatic learning circuits to elicit patterns of fMRI activity without requiring cognitive effort. This procedure, known as reinforcement learning or operant conditioning of fMRI patterns, has been successfully used to train the fMRI correlates of visual perception [64], confidence judgments [12], facial preference [63], color perception [3], and fear [40]. The mechanisms underlying this learning process are unclear. Because we had more factors to examine than would be feasible with the MRI scanner, we constructed a fully computational model to address how this process may occur. This allowed us to quickly and effectively evaluate whether continuous or intermittent feedback would more reliably elicit this type of automatic learning. Thus, we were able to use the same simulated neurofeedback environment to examine both cognitive and automatic learning mechanisms, demonstrating its efficacy as a neurofeedback research testbed.

2.2 Results

2.2.1 Using cognitive strategies to activate simulated visual cortex

We created a real-time feedback environment where human participants made cognitive decisions to maximize a simulated neurofeedback signal. Mental imagery is the most commonly used cognitive strategy in neurofeedback [67], but is difficult to quantify, varies between subjects, and cannot be reported on a second-to-second basis. Here we used measurable overt motor output as a proxy for mental strategies. Human participants used one of two buttons to rotate a grating image clockwise or counter-clockwise (Fig 2.3A). This grating image directly stimulated our V1 model based on its orientation. During each trial, participants were instructed to find a target orientation between 0° and 180° by rotating the grating. Participants found these targets by interpreting a decoded fMRI-like feedback signal indicating the probability that the grating was aligned with the target orientation. The signal was decoded using an 8-way sparse logistic regression classifier [46] trained on simulated data from each of the eight tuned orientations of our V1 model (Fig 2.2A). In this way, we operationalized a mental imagery strategy as a simple motor decision that influenced a model of V1 neural activity. In contrast to more implicit neurofeedback learning experiments [64, 3], the feedback received by participants was directly related to the physical properties of the grating stimulus which participants viewed. Thus, it eliminated any ambiguity about the relationship between their strategy choice and the feedback signal other than temporal delays and blurs. We address the additional complexity of implicit learning in our automatic learning simulations,

which did not explicitly use the grating stimulus to generate feedback signals.

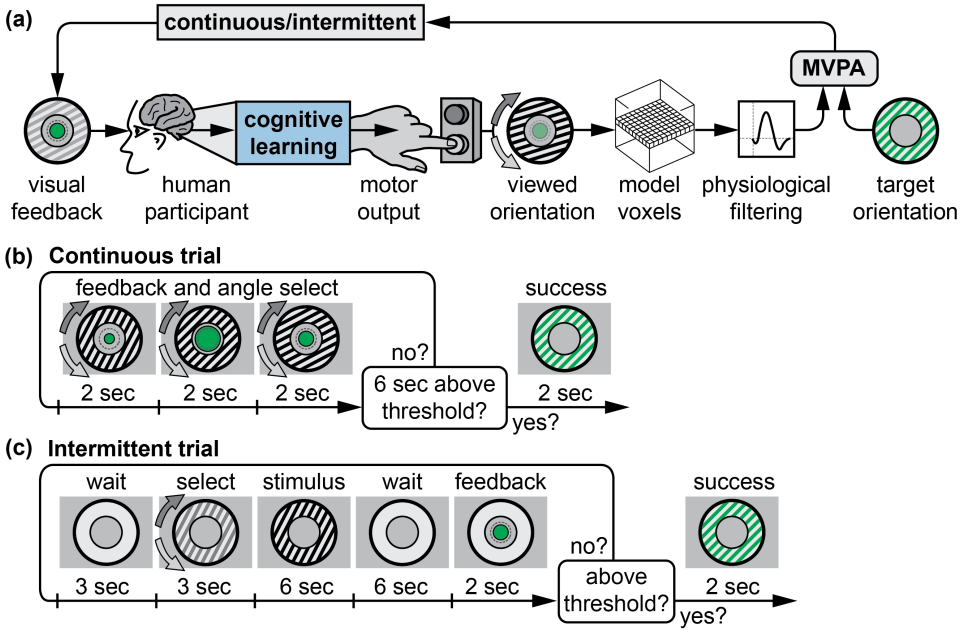

Figure 2.3: **Cognitive learning of neurofeedback signals. (A)** In this simulation, participants influence simulated neural activity by using a motor strategy to stimulate our model of V1. Button presses rotate a grating, which then induces activity in the V1 model. After physiological filtering, the resulting volume is decoded based on a target orientation and presented as visual feedback either continuously or intermittently. **(B)** For continuous feedback target searches, participants are able to continuously update the grating orientation, and the feedback signal updates every 2 seconds. **(C)** For intermittent feedback target searches, participants select one orientation each trial and receive summarized feedback at the end of each trial.

Participants were assigned into continuous and intermittent feedback timing groups (Fig 2.3B,C) and exposed to all of the simulated physiological filters (Fig 2.1E) to examine how these modified or impaired participants' cognitive strategies. In addition to our hypothesis that the hemodynamic response should

be more difficult to learn than isolated delay or blur responses, we also hypothesized that participants in the intermittent feedback group would find targets faster since this feedback timing makes the credit-assignment problem easier by accounting for the hemodynamic delay.

2.2.2 Continuous feedback is superior to intermittent feedback for simple cognitive strategies

In our cognitive simulation, we were able to create a one-dimensional cognitive strategy (selection of grating orientation) that could be quickly understood by participants. In this setting we found that in contrast to our hypothesis, the continuous feedback group was able to find targets faster than the intermittent feedback group for the HRF, blur, and delay physiological filters (Fig 2.4). The largest difference was found in the blur condition ($t_{(36)}$=11.06, $p<0.0001$), with a large difference also found in the HRF condition ($t_{(36)}$=4.564, $p<0.0001$). The delay condition was the most similar between continuous and intermittent conditions, but continuous feedback was still significantly better ($t_{(36)}$=2.363, p=0.0237).

These results show that if participants can directly influence the feedback signal through simple action choices, they are able to rapidly learn its dynamics and can perform better than those receiving intermittent feedback. This suggests that feedback of physiological responses that delay or blur the underlying neural activity can be successfully learned through cognitive means with a continuous feedback signal, as long as an effective strategy (i.e. a specific,

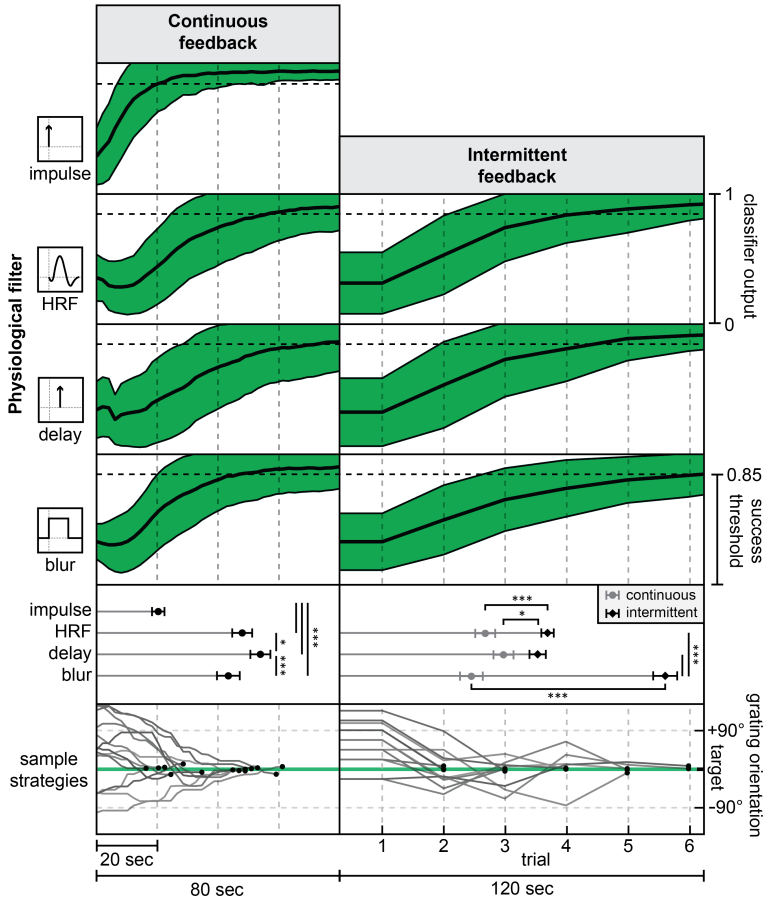

Figure 2.4: **Cognitive learning curves.** Learning curves were constructed by combining all target searches over all participants for each physiological filter. Plots in green show the mean classifier output (+/-s.d.) over the course of each target search. Because a new target was selected as soon as the current target was reached, all time points after success were simulated using randomly generated volumes at the target +/-5°. For means (+/-s.e.) of time to target for continuous (circles) and intermittent (diamonds) feedback, stars indicate significant differences at $p<0.05$ (*) and $p<0.001$ (***). In the sample strategy plots, the grating orientation for all HRF target searches from one participant (continuous: participant #3; intermittent: participant #9) are plotted relative to the target, with black circles indicating the time at which the target was reached.

well-defined behavior) is known to the participant. It is important to note that these conclusions may not generalize to explicit imagery tasks where many and more complex cognitive strategies could be used, when there are interdependencies between these strategies, or when the signal to noise ratio (SNR) of the neural signal is poor. For instance, in a study concluding that intermittent feedback was superior [37], the cognitive strategies employed by participants may not have been effective, and automatic processing of the intermittent feedback may have occurred in parallel to enable superior self-regulation compared to continuous feedback.

2.2.3 Physiological signal properties impact neurofeedback performance

Physiological filters also affect learning rate within each of the continuous and intermittent feedback conditions (Fig 2.4). In the case of continuous feedback, the impulse condition was found to be significantly easier to learn than the HRF (Tukey's HSD, $p<0.0001$), delay ($p<0.0001$), and blur conditions ($p<0.0001$). The pure delay condition was significantly more difficult to learn than both blur ($p<0.0001$) and HRF ($p=0.0305$). We also found a trending, non-significant effect suggesting that blur is slightly easier than HRF ($p=0.153$). For continuous feedback, an instantaneous neurofeedback signal derived from an impulse response filter was the easiest signal to learn. The HRF physiological response was also significantly more difficult to learn than the impulse response. The isolated delay and blur responses put the HRF result in context: a pure delay was even more difficult to learn than HRF or blur. The increased

difficulty of the delay physiological response conflicts with our hypothesis: we expected the HRF, which is a combination of delay and blur, to be the most difficult to learn. However, these results can be explained by the amount and timing of the contingent information received with each physiological response. For the impulse, participants receive 100% of the feedback information within 2 seconds. For blur, participants receive 20% of this information within 2 seconds, with the remainder of the information accumulating over the subsequent 10 seconds. The HRF filter provides no immediate information, but instead provides smeared and sluggish information over the next 6 seconds. The delay response gives no information at all until 6 seconds after the underlying neural activity has occurred. To summarize, it appears that the sooner that any neurofeedback information (even from partial or degraded signals) reaches the participant, the sooner they are able to adjust their cognitive strategy to find the target more quickly.

For intermittent feedback (Fig 2.4, right), the blur condition resulted in significantly worse performance compared to HRF (Tukey's HSD, $p<0.0001$) and delay ($p<0.0001$). There was no significant difference between the HRF and delay conditions in the intermittent feedback case ($p=0.672$). An artefact in the intermittent feedback calculation caused this sharp drop in performance with the blur response. The 6-sec stimulus period and subsequent 6-sec feedback calculation period of the intermittent feedback paradigm are well-matched to the HRF and delay responses, but not to the 10-sec moving average of the blur response. For the same grating orientation stimulus, the blurred response

resulted in a lower peak classifier output on average during the feedback calculation period. This meant that participants needed to be more accurate to reach the feedback signal success threshold. This shows that neurofeedback performance can be degraded if intermittent feedback timing and calculation are not well-matched to the physiological response properties of the signal being measured.

2.2.4 Automatic neurofeedback learning: strengthening neural patterns using reinforcement of spontaneous activity

While we found continuous feedback to be superior to intermittent feedback for cognitive strategies, this need not be true for all fMRI neurofeedback studies. A major drawback of our cognitive learning experiments is that they assume a static relationship between stimulus and brain activity. They effectively bypass the complexity of the brain by providing a direct pathway between stimulus and feedback signal in the form of a visually-presented grating. This is equivalent to a participant having a set of mental strategies that consistently map onto patterns of neural activity and that can be recalled as easily as pressing a button. This is clearly unrealistic if the trained neural circuit has no clear associated cognitive strategy or participants need to be kept unaware of the experimental manipulation. In these cases, implicit or automatic neurofeedback strategies must be used.

If no voluntary action or external stimulus influences neural activity, then we are faced with the challenge of controlling a neural signal that is driven by

unconstrained cognitive states (e.g., mind-wandering) along with a contribution from spontaneous neural activity. Over time, participants should be conditioned to elicit the desired pattern of activation whenever they anticipate a neurofeedback signal or when presented a conditioned cue. We cannot examine this phenomenon with human participants unless we use a real neural signal. Instead, we constructed a computational model that started with purely random, spontaneous activity patterns and learned to elicit desired activity through reinforcement provided by an MVPA classifier that was trained to recognize a desired pattern (i.e. simulated activity patterns corresponding to a stimulus). This model of automatic learning (Fig 2.5) followed a basic reinforcement learning structure [68]: changes in a feedback signal are used to reward or punish spontaneous neural activity, which is accumulated (integrated) over time.

Consider a vector of activity $\mathbf{a}[n]$ at time point (TR) n, which is a combination of spontaneous activity $\mathbf{a}_s[n]$ and learned (conditioned) activity $\mathbf{a}_c[n]$. Let $\mathbf{a}_s[n] = N \sim (0, \sigma_s)$, where spontaneous activity in each voxel is independent (we will later introduce spatial correlations). Given a matrix of classifier weights $W_{N_{voxel}xN_{class}}$ and a learning rate α, we can 'learn' the next conditioned activity, $\mathbf{a}_c[n+1]$ by observing the change in classifier output due to the current activity pattern. Defining $f[n]$ as the classifier output for the target (feedback signal) and $l[n]$ as the learning signal:

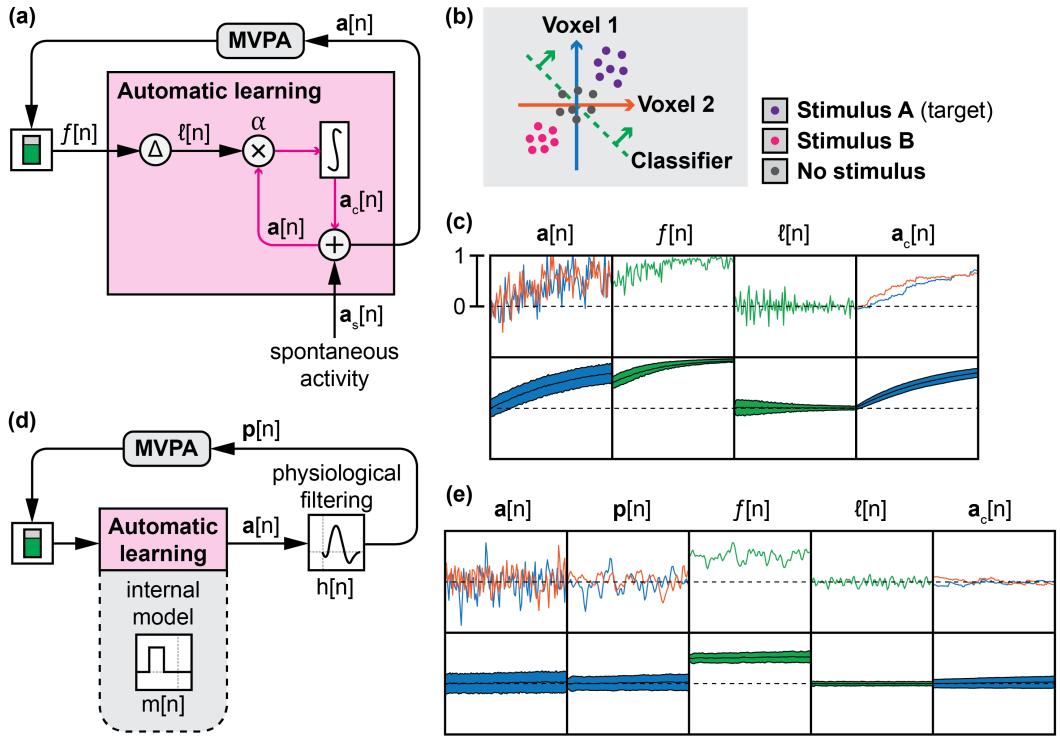

Figure 2.5: **Automatic learning of neurofeedback signals. (A)** Reinforcement learning is used to shape neural activity in the absence of delay. **(B)** A simple two-voxel neural model is used to demonstrate how our model of automatic learning can learn a pattern of neural activity associated with a stimulus. **(C)** Without delays, our model is able to learn the desired pattern of neural activity. The top row shows example data from one trial, while the filled plots on the bottom row show the mean and 50% confidence interval (CI) for each signal at each time point, averaged over 1000 simulated trials. **(D)** If significant physiological delays exist, then an internal model must exist to hold in memory underlying neural activity before it can be reinforced by the delayed feedback signal. **(E)** If no internal model exists, learning of neural activity filtered by the HRF does not occur.

$$
\begin{aligned}
\mathbf{a}[n] &= \mathbf{a}_s[n] + \mathbf{a}_c[n] \\
\mathbf{f}[n] &= softmax(W^T \mathbf{a}[n]) \\
f[n] &= \mathbf{f}[n]_{i=target} \\
l[n] &= f[n] - f[n-1] \\
\mathbf{a}_c[n+1] &= \alpha \cdot l[n] \cdot \mathbf{a}[n]
\end{aligned}
\tag{2.1}
$$

Where $softmax(\cdot) = e^{(\cdot)}/\Sigma e^{(\cdot)}$ ensures that the feedback signal represents the likelihood of the target class being observed. In this example, feedback is instantaneous to the underlying neural activity (e.g. the physiological response is an impulse), and spontaneous activity can easily be rewarded because the feedback and underlying neural activity are occurring at the same time.

Our next step was to test this automatic feedback learning structure in a simple simulation: a two-voxel brain with two classes of stimuli and a classifier weighting $W = \left[\begin{smallmatrix} 1 & -1 \\ 1 & -1 \end{smallmatrix}\right]$ (Fig 2.5B). We used a learning rate $\alpha = 1$ and spontaneous activity $\sigma_n = 0.25$. Using Eq (2.1), we expectedly found that given a desired activity pattern, the desired activity was elicited (Fig 2.5C). However, we hypothesized that this simple learning rule would be unable to learn the underlying neural activity if the feedback signal was filtered by some sort of physiological response such as the HRF before being measured and presented as feedback (Fig 2.5D). Indeed, we found that this physiological filtering impairs learning (Fig 2.5E). We are aware of models that exist for automatic learning of near-instantaneous electrophysiological signals [48], but not for signals with a time delay similar to the HRF. For these longer delays, we posit that an internal model of the relationship between underlying neural activity and feedback signal must exist to solve the credit-assignment problem by holding in memory the underlying neural activity until the feedback signal can be presented (Fig 2.5D, Fig 2.6A). This internal model is purely temporal and has no spatial awareness. All voxel activities are rewarded or punished equally by the feedback signal at

specific time points in the past, where the weighting of time points is defined by the internal model. This is analogous to a sliding window memory of whole-brain neural activity [60] that a delayed feedback signal is able to reward or punish.

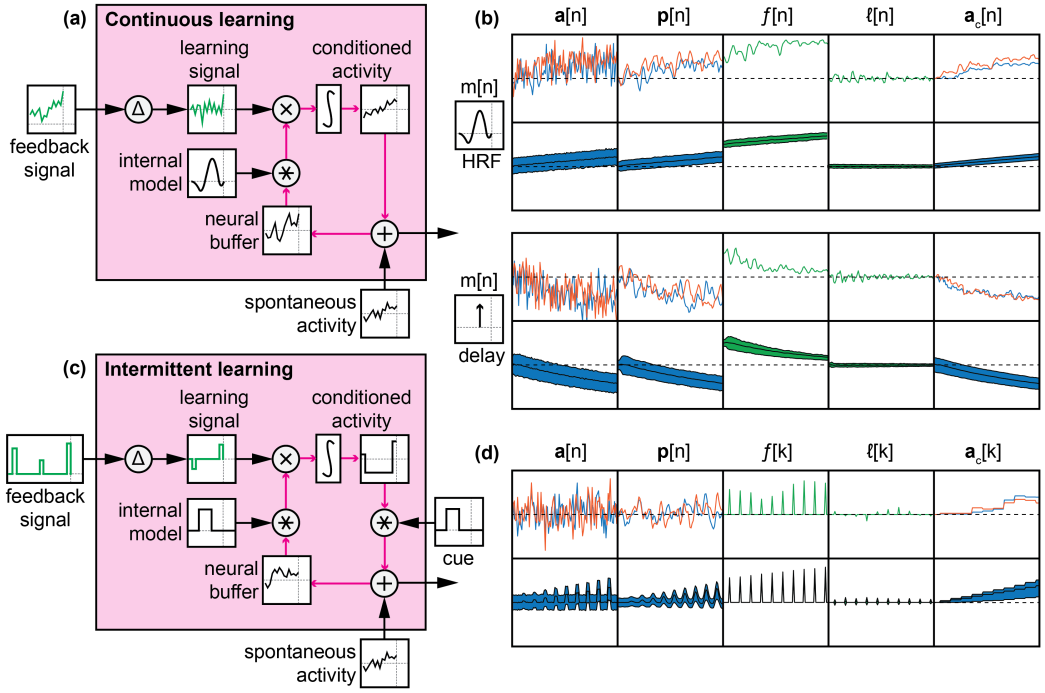

Figure 2.6: **Automatic learning of continuous versus intermittent neurofeedback signals. (A)** For continuous learning, a buffer of neural activity is kept in memory and filtered by the internal model. **(B)** In continuous learning, learning can occur when the internal model accurately matches the underlying physiological response. However, with a delay internal model, anti-learning occurs when the underlying neural activity is filtered by the HRF. **(C)** For intermittent learning, a cue is used to gate the conditioned activity. **(D)** Intermittent feedback allows trial-by-trial learning of underlying activity that is filtered by the HRF.

To simulate this internal model, we must augment Eq (2.1) with $h[n]$ as the delayed or blurred physiological response, $m[n]$ as the internal memory

model, and $\mathbf{p}[n]$ as the delayed or blurred physiological activity:

$$\begin{aligned}\mathbf{p}[n] &= \mathbf{a}[n] * h[n] \\ \mathbf{f}[n] &= softmax(W^T \mathbf{p}[n]) \\ \mathbf{a}_c[n+1] &= \alpha \cdot l[n] \cdot (\mathbf{a}[n] * m[n])\end{aligned} \tag{2.2}$$

If we assume a maximum length L of the physiological response and internal model, we can expand Eq (2.2) as follows:

$$\begin{aligned}\mathbf{a}_c[n+1] &= \alpha\big(f[n] - f[n-1]\big) \cdot \sum_{n=-L}^{0} \big(\mathbf{a}[n] m[-n]\big) \\ f[n] &= softmax\left(W^T \sum_{n=-L}^{0} \big(\mathbf{a}[n] h[-n]\big)\right)_{i=target}\end{aligned} \tag{2.3}$$

Although the $softmax$ calculation prevents further meaningful simplification of these equations, we can see from Eq (2.3) that matching $m[n]$ to $h[n]$ should help reduce the learning problem toward a summation of impulse learning problems (e.g. those in Eq (2.1)). Indeed, if we include an internal model that matches the underlying physiological response, such as an HRF internal model for the HRF physiological reponse, we see that learning can now occur (Fig 2.6B, top). However, if the internal model is not perfectly matched to the actual neural response, such as a delay internal model, we see that it is possible for anti-learning to occur: the opposite pattern of desired activity is learned (Fig 2.6B, bottom). This result is of critical importance because participants' internal models cannot be verified and because a 'pure delay' model is typically one of

the verbal instructions given to participants to describe the hemodynamic lag [67]. Therefore, with continuous feedback, there is risk that an incorrect internal model will be generated, leading to poor learning or even anti-learning of the neurofeedback signal.

So far, we have only considered the problem of continuous feedback. We initially hypothesized that intermittent feedback would be superior to continuous feedback, and although this was not the case for cognitive strategies, we will now examine intermittent feedback in the context of automatic learning. For intermittent feedback, learning during each trial k with cue period $n_{c,1} \leq n \leq n_{c,2}$ and subsequent pre-feedback wait period $n_{w,1} \leq n \leq n_{w,2}$ takes the following feedback structure:

$$\begin{aligned}
\mathbf{a}[k] &= \frac{1}{n_{c,2} - n_{c,1} + 1} \sum_{n=n_{c,1}}^{n_{c,2}} \big(\mathbf{a}_s[n] + \mathbf{a}_c[n]\big) \\
f[k] &= \frac{1}{n_{w,2} - n_{w,1} + 1} \sum_{n=n_{w,1}}^{n_{w,2}} f[n] \\
l[k] &= f[k] - f[k-1] \\
\mathbf{a}_c[k+1] &= \alpha \cdot l[k] \cdot \mathbf{a}[k]
\end{aligned} \tag{2.4}$$

Using this intermittent feedback structure (Fig 2.6C), the learning problem in Eq (2.4) is roughly reduced to the impulse learning problem of Eq (2.1), albeit on a slower time scale. Using the HRF physiological response in our automated learning simulations, a cue period of 3 TRs, and a subsequent wait period of 3 TRs, we found that intermittent feedback also led to successful learning (Fig

2.6D).

2.2.5 Activating simulated visual cortex using reinforcement of spontaneous neural activity

Given that our automatic learning model worked to elicit a desired pattern of activity in a simple two-voxel model, our next goal was to train activation patterns in our full V1 model without directly stimulating it with grating images (i.e. a simulation of the experiment performed by Shibata et al. (2011) [64]). Using the same neural model as the cognitive experiment (which contains spatial noise correlations typical of fMRI), we constructed a 3-way sparse logistic regression classifier (Fig 2.7A) and aimed to elicit the pattern of activity associated with a grating oriented at 10°. Our comparison of continuous versus intermittent feedback was similar to the cognitive experiment, with continuous feedback provided every 2 seconds (Fig 2.7B), and a cue replacing the direct stimulus during intermittent trials (Fig 2.7C). We then aimed to test how different internal models affected automatic learning. Specifically, we addressed whether learning could occur with different delayed or blurred underlying physiological responses, and if so, how accurate did the internal model need to be? In addition to a general hypothesis that intermittent feedback would be superior, we hypothesized that for continuous feedback, matched filter-model combinations (e.g. HRF-HRF) would produce the best learning, whereas incongruent filter-model combinations (e.g. HRF-delay) would produce the least learning.

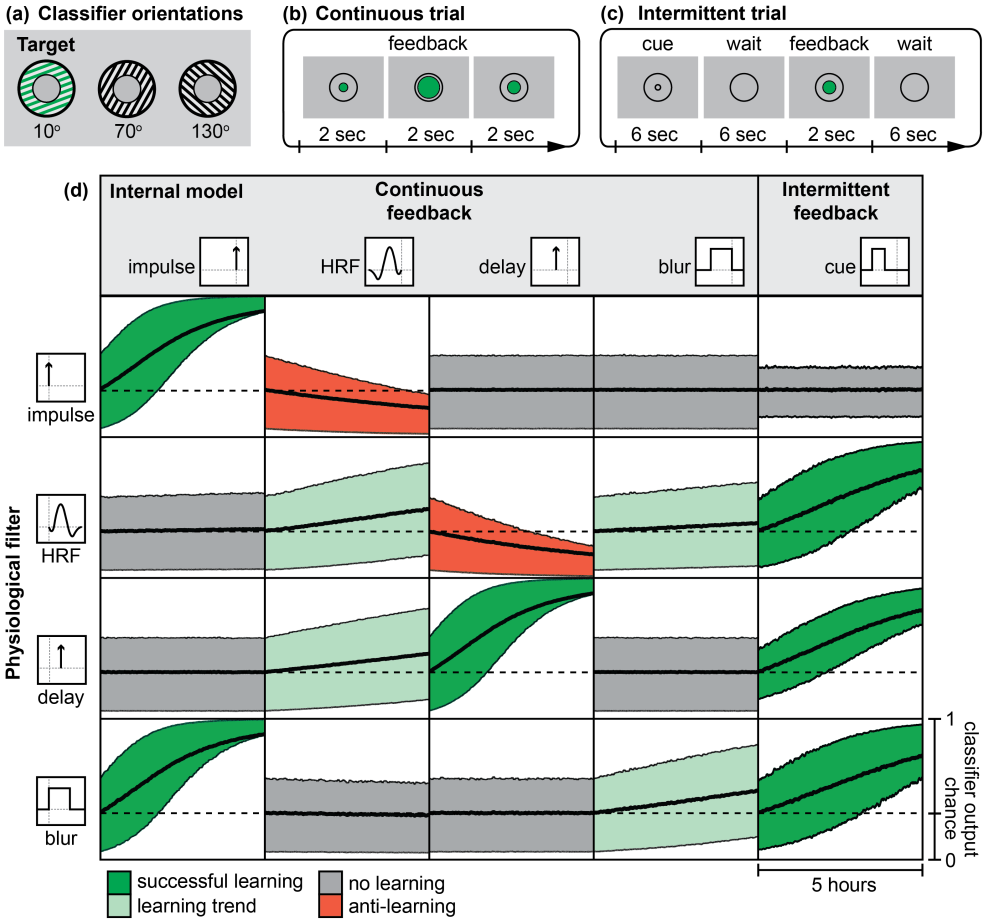

Figure 2.7: **Automatic learning of grating patterns in simulated V1. (A)** A 3-way sparse logistic regression classifier was used, with feedback provided from the 10° classifier output. **(B)** For continuous trials, feedback was provided to the learning model every 2 seconds. **(C)** Intermittent trials followed a cue-wait-feedback structure. **(D)** Learning curves were generated by averaging the classifier output at each time point over 1000 simulated participants for each condition. Filled plots indicate the mean and 50% confidence interval (CI) for each time point, which was further filtered using a 200-sec moving average filter (about 1% of the total time course) for graphical presentation purposes. Chance is indicated at 0.33. Plots are colored according to feedback success.

2.2.6 Automatic learning of neurofeedback signals requires an accurate internal model

Our automatic learning simulations show that successful learning in the absence of cognitive strategies depends on the underlying physiological response and the internal model used to interpret that temporal response (Fig 2.7D). For example, for the HRF physiological response, successful learning was found with a cue model. Moderate learning was found with HRF and blur models, with HRF leading to quicker learning than blur. No learning was found with an impulse model, and a delay model resulted in anti-learning. These results align with our simple two-voxel model (Fig 2.6). This confirms that increased dimensionality and moderate spatial noise correlation do not have an effect on the working principle of our automatic learning model.

Contrary to our hypothesis, we found that with a continuous feedback signal, matched filter-model combinations only led to successful learning for impulse-impulse and delay-delay combinations. The incongruent blur-impulse filter also showed successful learning and was superior to the matched blur-blur model. We believe this can be explained by the temporal dependency of the system: the learned signal is integrated over time, so successful spontaneous activity should be captured and reinforced as soon as possible. With the impulse internal model, as soon as successful activity occurs, it is captured by the blur filter and is immediately reinforced. With a blur internal model, this successful activity is only reinforced at 20% strength (averaged across the previous 5 TRs, or 10 sec of simulated neural data), and becomes lost in the noise. Another

temporal relationship may also explain why a delay internal model does not result in learning of the blur filter, whereas an impulse model does. Both of these internal models sample one time point from the blur filter, and all 5 TRs (10 seconds) are weighted equally. However, our model only learns when there is a change in the feedback signal. When successful activity occurs, the change in feedback signal is immediately captured by the blur physiological response filter and reflected as a change in the feedback signal that an impulse internal model can learn from. If a delay internal model is used instead, there is no change in feedback signal at the 3 TR delay, and thus no learning occurs.

For intermittent feedback, we see successful learning for the HRF, delay, and blur filters. Indeed, this feedback schedule has been successful for automatic learning of fMRI acivity patterns [64, 63]. These results suggests that the same intermittent feedback schedule can be used to learn a variety of physiological responses as long as the neural activity in the cue period is reliably recorded during the wait period.

2.2.7 Automatic learning of spatial patterns depends on spontaneous activity correlations

While our model was able to learn to achieve a large classifier output, it is possible that this occurred simply due to activity in one or two voxels. To address this concern, we performed an additional simulation with visualizable activity patterns (Fig 2.8). The 200 tuned voxels and 3 classifier weight maps from our V1 model were randomly placed onto a 20x20 (400-voxel) surface.

Conditioning was performed using the hrf-cue filter-model combination from Fig 2.7D, as is common in decoded neurofeedback experiments [64]. Over 1000 simulated participants using the same noise parameters as Fig 2.7 (e.g. without spontaneous activity correlations), we found that the classifier output was indeed driven by a distributed pattern of activity. However, this activity correlated more strongly with the classifier weights associated with the target orientation ($r = 0.44$) than the true orientation-associated pattern ($r = 0.15$). This pattern of correlations was also found in the two non-target orientations: larger magnitude correlations with classifier weights ($r = -0.20, -0.22$) relative to the true orientation patterns ($r = -0.08, -0.07$). These negative correlations indicate that the patterns associated with non-target orientations are punished, which is consistent with the $softmax$ operation of the classifier capturing information from all three classifier weight maps.

Weak correlations with the true orientation patterns are likely related to the sparsity [46] of the classifier: the classifier does not select all voxels associated with the true orientation pattern, so how could the model learn activity in these unselected voxels? True patterns of spontaneous activity in V1 are not truly random: they tend to contain information associated with visual attributes [39]. If orientation signals are present in the spontaneous activity, then our model should be able to learn activity in voxels not selected by the classifier. To test this hypothesis, we introduced a noise model that was a half-and-half mixture of random Gaussian noise and a random orientation signal between 0° and 180°. This random orientation signal ensured that while visual attributes

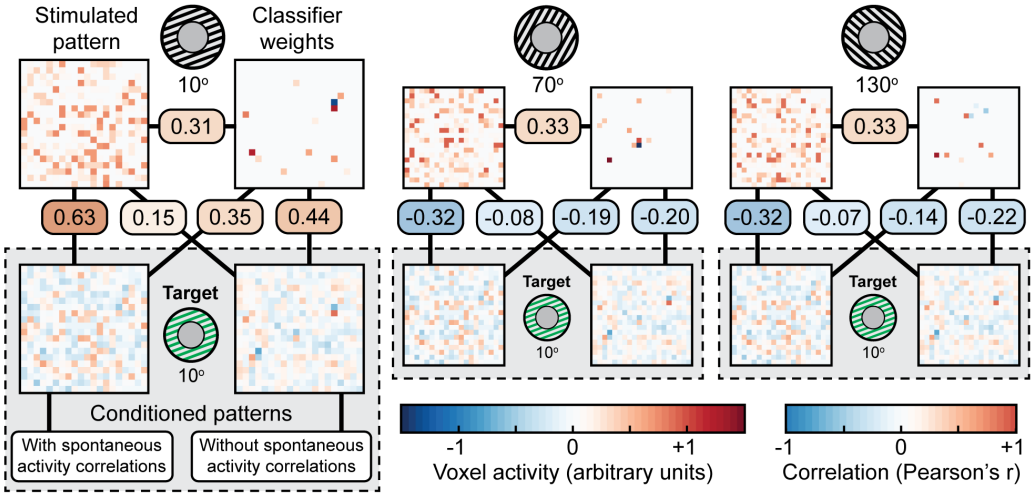

Figure 2.8: **Conditioned patterns of activity with and without spontaneous activity correlations.** True orientation-associated patterns, classifier weight maps, and conditioned activity patterns were projected onto a 2D surface. Patterns of activity were distributed across voxels and were not dominated by one or two voxels. For each of the three classifier orientations (Fig 2.7A), the true underlying pattern associated with the stimulus is shown (without spontaneous activity added), as well as its corresponding classifier weight map. 1000 patterns were conditioned to purely random Gaussian noise ('without spontaneous activity correlations'), while 1000 patterns were conditioned with a mixture of Gaussian noise and a random orientation signal ('with spontaneous activity correlations'). Feedback was provided from the 10° classifier output for both types of conditioning. One example of each type of conditioned pattern is shown. The displayed correlations are the mean correlation across all 1000 patterns.

were included in the spontaneous activity, it did not have any bias toward the target orientation. Using the same conditioning procedure as before, we found that this noise model resulted in conditioned patterns that had much stronger correlations with the true target pattern ($r = 0.63$) and weakened correlations with the target classifier weight map ($r = 0.35$) (Fig 2.8).

2.3 Discussion

We simulated fMRI activity in visual cortex to determine how feedback timing affects learning of neurofeedback signals with different physiological responses and self-regulation strategies. Our first experiment had human participants find hidden visual targets (oriented gratings) using only simulated neural activity as a feedback learning signal. We used four physiological filters in this experiment: instantaneous feedback, the canonical HRF of fMRI, and isolated delay and blur filters. One group was exposed to continuous feedback, while another saw intermittent feedback. In a second experiment, we fully simulated the automatic learning of neurofeedback signals, examining how continuous and intermittent feedback could be used to induce a pattern of activity in simulated visual cortex without stimulus presentation. We found that continuous feedback was best for cognitive strategies, whereas intermittent feedback was better for automatic learning. For cognitive learning of neurofeedback, we found that all properties of hemodynamics impair neurofeedback learning, but the delay of the continuous feedback signal affects learning more than the blur. For automatic learning, we found that intermittent feedback was able to absorb differences in hemodynamic properties to facilitate learning, whereas a precise and accurate model of the hemodynamic response was necessary for learning with continuous feedback.

Our analyses isolated cognitive and automatic learning of a simulated neurofeedback signal under ideal conditions. In practice, neurofeedback experiments are often underspecified, and may rely upon some combination of both

learning techniques [66]. Because of the interaction between feedback timing and learning technique, our results suggest that either cognitive or automatic learning strategies should be chosen before feedback timing is scheduled in an fMRI neurofeedback experiment. Furthermore, while the relative effects of blur and delay shown in our cognitive results apply to all neurofeedback studies with a prescribed cognitive strategy, the absolute performance we reported (e.g., time-to-target in a search for a hidden target neural activity pattern) does not apply to the majority of fMRI neurofeedback studies because of the simple, unidimensional nature of our cognitive strategy and the arbitrary SNR that was used. Increasing noise and allowing for more complex, multidimensional strategies could drastically increase time-to-target in our simulation. The static relationship between stimulus and brain activity was a further simplification that may not hold true when the 'stimulus' is a complex cognitive strategy chosen by a participant. Importantly, these pitfalls do not apply to automatic processing: strategy is not chosen by the participant, and noise due to spontaneous activity is displayed as useful information in the feedback signal. Therefore, unless a simple, known cognitive strategy will reliably elicit the desired neural activity, our results suggest that automatic processing is more likely to result in successful learning of fMRI neurofeedback signals.

Our automatic learning model answers the question: given an internal model of the temporal dynamics of the feedback signal, how is the feedback signal learned? It does not attempt to explain how this internal model may be generated or adapted over time. While the feedback/wait/cue structure of inter-

mittent feedback is a plausible mechanism to create a stable internal model that is agnostic to the actual temporal characteristics of the underlying physiological response, it is unclear how an internal model would be created for a continuous feedback signal. For example, given verbal instructions about the blur or delay of the feedback signal, their translation into a filter applied to an internal memory buffer of neural activity is unknown. In the absence of instruction, animals effectively use a short time scale, near-impulse model to self-regulate continuous electrophysiological signals (For a detailed model involving spiking neurons, see Legenstein et al. (2008) [48]). For longer time scales, it is widely accepted that conditioning can occur as long as the delay to reinforcement is predictable [24]. However, without a predictable cue structure, a pessimistic viewpoint would argue that the impulse model is used by default for continuous feedback signals, which is ineffective for learning feedback signals that are significantly delayed or blurred.

There is evidence to show that a neural representation of time exists to store neural activity in memory [60]. This temporal representation becomes less accurate the longer the delay, but nevertheless provides a mechanism for a continous-time internal model. The problem is then still: which time delay does the brain choose to reinforce? The difficulty of creating an appropriate internal model may explain the inability for some participants to gain control over continuous fMRI neurofeedback signals, and could therefore underlie the “non-responder" challenge in human neurofeedback [28]. Our simulation results are inconsistent with the results of Ramot et al. (2016) [57], who used

continuous feedback of the hemodynamic response to shape neural activity in the absence of awareness of the meaning of the feedback signal. It would appear that either participants were able to generate a working internal model of the temporal characteristics of the feedback signal (e.g. the blur or HRF internal models applied to the HRF physiological response in Fig 2.7D) in the absence of external cues, or these results were simply obtained by chance without any true neuromodulation due to the feedback signal. Another pitfall of using continuous feedback in automatic learning is that an incorrect internal model can result in anti-learning. For example, the impulse-HRF and HRF-delay models end up worse than chance (Fig 2.7D). Verbal instructions may help participants tune their internal models, but given that one of the common instructions (a 6-second delay internal model) resulted in anti-learning in our simulation, this seems risky compared to simply scheduling feedback intermittently.

Our automatic learning simulations also shed light on the debate regarding how patterns of activity can be learned in a high-dimensional voxel space [35, 62]. Huang (2016) argues that because participants do not have cognitive access to the voxel space, the dimensionality of this space is too large for participants to reliably discover an effective cognitive strategy to activate the desired pattern. Shibata et al. (2016) counter-argue that the dimensionality of the search space is actually much smaller than the voxel space would suggest due to correlations in V1 activity. We provide an alternative explanation to both arguments. First, cognitive access to the voxel space is not required since automatic learning circuits can reward the underlying neural activity without participant

awareness. Second, a global (whole-brain) reward signal allows complex activity patterns to be conditioned, even with high-dimensional spontaneous neural activity patterns.

The neurofeedback simulation framework reported here is intended as a proof of concept: we started with a simplified model of V1 for clarity. Looking forward, this model has two major limitations. First, our noise model did not include any measurement noise, so all simulated activity was a result of spontaneous activity and not error in the simulated measurement. Measurement noise would almost certainly have a negative impact on learning, but the ratio of signal/spontaneous/measurement noise in fMRI is difficult to quantify [78] so we chose to simplify our model and leave open the potential to improve its specificity in future iterations. Our noise was also Gaussian with local spatial correlation. This noise model is not sophisticated enough to capture the true complexity of visual cortex: we know that correlational structures exist within spontaneous activity in V1, and that these patterns tend to correlate with basic visual attributes [39]. We also know that using neurofeedback signals that match patterns of spontaneous activity are easier to learn [59]. Therefore, adding a more realistic correlational structure to our noise model should not affect the qualitative relationship between physiological responses and internal models, but rather it should show that patterns that commonly occur spontaneously will be easier to learn through neurofeedback. Indeed, when we added random visual attributes to our spontaneous activity model (Fig 2.8), we found that conditioned activity patterns more closely matched the target orientation pattern compared to

conditioning with completely random spontaneous activity. Second, our spatial capture model was based on meta-parameters from prior work [38]. An advanced spatial capture model, such as one recently developed by Kriegeskorte and Diedrichsen (2016) [45], could be used as a basis for the simulated neurofeedback signal. This capture model shows that shifts in voxel sampling over finer-grained neural activity can bias the recorded representational structure of stimuli. Such a model could help determine whether neurofeedback is feasible given a specific neuroimaging method and targeted neural pattern.

Overall, our model demonstrated an important contrast between cognitive and automatic neurofeedback strategies, suggesting that different self-regulation mechanisms prefer different feedback schedules. These findings have significant implications for any experiment involving the feedback of delayed or blurred signals, and have direct applications for the design of neurofeedback schedules and instructed strategies for future fMRI neurofeedback experiments. Furthermore, the simulation framework provides a basis to evaluate and optimize the design of such experiments before they are performed with real neuroimaging data.

2.4 Methods

2.4.1 Ethics statement

This study was approved by the University of Texas Institutional Review Board. Written informed consent was obtained from the participants.

2.4.2 Participants

Forty-eight healthy participants (27 female; average age 20.34 years, SD=3.08) were recruited for the experiment. Participants were randomly assigned into 2 groups: 24 received continuous feedback and 24 received intermittent feedback.

2.4.3 Apparatus

Participants were seated at a computer (21.5" iMac) and used the arrow keys on a standard keyboard to perform the experiment. Data were sampled and displayed at 60 Hz using Matlab and Psychtoolbox 3 on Mac OS X. No neuroimaging apparatus was required.

2.4.4 Model parameters: voxel-based V1 captured by simulated fMRI

Our model of V1 (Fig 2.2a) is based on meta-parameters extracted from Kamitani and Tong (2005) [38]: a 1000-voxel cube of 3x3x3mm voxels, with 20% of voxels tuned to grating orientation (2.5% to each of 8 orientations) and 80% of voxels untuned. The tuning curve for each voxel is a decaying exponential, with full output (arbitrary units) at the tuned orientation, decaying to 1/16 output at the orthogonal orientation. Underlying neural activity is generated according to the orientation of the stimulus and the corresponding voxel tunings. Spatially correlated spontaneous activity (Gaussian random field with 5mm kernel) is added to this tuned activity and the result is convolved in time with a physiological response filter.

The four physiological responses (Fig 2.1E) are sampled at 0.5Hz, corresponding to the 2 second time repetition (TR) of standard fMRI capture. Therefore, the impulse samples one TR of activity with no delay, the delay samples one TR of activity with a 3-TR delay, and the blur averages over the previous 5 TRs. The HRF filter is a weighted average of the previous 15 TRs of activity, according to the canonical fMRI BOLD response. All filters were normalized such that the sum of their weights equalled one.

2.4.5 Model parameters: cognitive learning

The classifier used to decode cognitively-elicited simulated fMRI patterns in real-time (Fig 2.2B) used a sparse logistic regression classifier [46] because this technique has been successfully applied to fMRI data from V1 [86]. To train the classifier, we simulated 800 training examples (100 each of the 8 tuned orientations: 0°, 22.5°, ..., 157.5°) using a voxelwise signal-to-noise ratio (SNR) of 2 (tuning curve peak=1; spontaneous activity σ_n=0.5). These parameters were chosen to approximate the results from a two-hour-long pattern localizer experiment [38].

We generated simulated brain activity online using the predetermined grating orientation-voxel activation relationship. For each time repetition (TR=2 seconds), the mean grating orientation during that period was input to the model. Through piloting, we found that with a realistic SNR of 2, participants often reached targets by chance rather than through interpretation of the feedback signal. We therefore increased the SNR of all voxels (tuned and untuned) to

10 (spontaneous activity σ_n=0.1). This increased the reliability of the feedback signal for participants so that we could more readily examine the temporal characteristics of the physiological signals.

The simulated neurofeedback signal was calculated using a weighting of the eight decoded orientation probabilities from the classifier. Specifically, the feedback signal was calculated by the dot product of the vector of classifier probabilities and a tuning curve, where the tuning curve was a decaying exponential circularly shifted to align its peak with the target orientation. This resulted in a smooth, gradually increasing feedback signal throughout the stimulus orientation range, instead of one that remained low and then peaked sharply at the target orientation. For example, if the classifier was 100% confident that the grating was 22.5° away from the target, the classifier would output a 0% probability for the target orientation, even though the participant was near the target. By using the dot product of the tuning curve and the raw classifier output for all orientations, the simulated neurofeedback signal for a grating 22.5° away from the target is 50% (instead of 0% if only the classifier output for the target orientation was used). If the classifier was 100% confident the grating was 45° away from the target, this dot product would instead output 25%, and so on. Importantly, the scalar output of this dot product always lies between 0 and 1, so it can easily be displayed on a thermometer without additional scaling.

To determine whether participants had reached the target, a threshold of 85% classifier output at the target was selected because this corresponded to roughly 5-10 degrees of grating orientation error from the target (depending

on noise) and was feasible for participants to reach during piloting of the experiment. If the average classifier output over 3 consecutive TRs preceeding a feedback period exceeded this threshold, the trial was considered successful and a new trial began.

2.4.6 Procedure: visual display

We used a square-wave grating, 50% contrast, 0.5 cycles/degree, visible from 4-20° of visual angle. A black fixation circle was centered with a diameter of 0.5°. The green feedback circle was linearly mapped from 0-100% classifier output to 0.6-3.5°. A grey circle was displayed at 85% (3.065°) to indicate the success threshold. On training trials, the target was shown to participants so that they could learn how the feedback signal behaved. On these trials, a target orientation grating was shown (square-wave, 50% contrast, 0.5 cycles/degree, 4.5°), appearing underneath the feedback circle but on top of the stimulus grating, slightly covering it.

2.4.7 Procedure: continuous feedback

Continuous target search timings are summarized in Fig 2.3B. Each continuous target search began with the grating oriented horizontally (0°). Participants rotated the grating image using either the left (counter-clockwise) or right (clockwise) arrow keys (Fig 2.3A). While either key was depressed, the grating rotated at a constant rate of 45°/second. The grating did not rotate if neither or both keys were pressed. The V1 model was updated every two seconds

based on the mean grating orientation over the previous two seconds. At each update period, the feedback circle expanded or contracted over 500ms from the previous value to the updated value to ensure a smooth visual display. If the average feedback signal exceeded the success threshold circle for three consecutive TRs, the target was considered reached and participants saw their grating orientation in grey overlaid with the true target orientation in green (Fig 2.3B).

Continuous target searches were organized into four blocks, with each block using one of the four candidate physiological filters. The first block was always the impulse condition, because this was the easiest condition and served as familiarization for participants. The next three blocks were the three other physiological filters: HRF, blur, and delay. Ordering of these three blocks was counterbalanced across participants. Each block began with three visible training targets at 45°, 90°, and 135°, so that participants could familiarize themselves with the feedback signal dynamics. This was followed by 14 hidden targets, randomly located at 0°, 22.5°, ..., 157.5°, with two targets per orientation. A self-paced rest period was provided between each block, with an indication that the feedback signal behavior was about to change. Each block lasted about 10 to 20 minutes, depending on participant ability and the difficulty of each physiological filter.

2.4.8 Procedure: intermittent feedback

Intermittent trial timings are summarized in Table 2.1, with non-accelerated timings illustrated in Fig 2.3C. Each intermittent target began with the grating oriented horizontally (0°), and participants had three seconds to select an initial orientation. During this orientation selection period, the grating was greyed out (25% contrast) and rotated at a constant rate of 60°/second according to participants' button presses. Rotation speed was increased relative to continuous feedback to allow for a full 180° of rotation during the 3 second adjustment period. Next, the stimulus was displayed at full contrast (50%) for a stimulus period whose duration depended on the feedback acceleration factor. Following a variable-length delay period (depending on feedback acceleration), feedback associated with the stimulus was presented for two seconds. The feedback signal was calculated by stimulating the V1 model with the selected orientation for 3 TRs (6 seconds), then averaging the feedback signal recorded in the following 3 TRs to account for the physiological delay. If the feedback signal exceeded the success threshold, participants saw their selected grating orientation in grey overlaid with the true target orientation in green (Fig 2.3C). If the feedback score did not reach the success threshold, a new trial with the same target began after a brief (depending on feedback acceleration) wait period. Starting from the second trial for a given target, the feedback display period began with a smooth 500ms update from the previous trial's feedback value. Intermittent trials were organized into seven blocks with nine targets each. Targets were randomly located at 0°, 22.5°, ..., 157.5°, with nine targets per orientation. The first three

targets of the first block had the target visible to familizarize participants. All remaining targets were hidden. A self-paced rest period was provided between each block.

Table 2.1: Intermittent trial timings

Acceleration	Select	Stimulus	Delay	Feedback	Wait	Total
Real-time	3 sec	6 sec	6 sec	2 sec	3 sec	20 sec
2x	3 sec	3 sec	3 sec	2 sec	2 sec	13 sec
6x	3 sec	1 sec	1 sec	2 sec	1 sec	8 sec

2.4.9 Procedure: accelerated intermittent feedback

We introduced and validated an accelerated intermittent feedback protocol to reduce experimental duration while preserving the trial-by-trial intermittent feedback signal characteristics. Accelerated intermittent trial timings are summarized in Table 2.1. Our validation used only the HRF physiological response filter. Targets were randomly and evenly assigned one of three trial timings: real-time, 2x accelerated, and 6x accelerated. The real-time timing corresponded to the required timing if a real physiological signal were measured: 6 seconds of stimulus, 6 seconds of waiting for the physiological signal to catch up, and 6 seconds between the end of feedback and the beginning of the next stimulus to allow the physiological signal to return to baseline. The 2x and 6x acceleration factor trials had the stimulus and subsequent wait period sped up accordingly. While these resulted in shorter trials (13s and 8s respectively), the trial-by-trial feedback signal was still simulated according to the real-time protocol, meaning that there was no difference in the trial-by-trial information observed by partic-

ipants. This allowed us to investigate whether performance was affected by delays between stimulus and feedback. Participants (n=10) were not informed about the different acceleration factors, which changed on a target-by-target basis but were constant for all trials on a given target. We constructed a linear mixed effects model of trials to target using feedback acceleration as a fixed effect and participant as a random effect. There was no significant effect of acceleration factor ($F=0.239$, $p=0.788$). Thus, all remaining intermittent feedback participants (n=14) were exposed to the 6x acceleration factor.

2.4.10 Procedure: intermittent feedback with different physiological responses

In this intermittent feedback protocol, the HRF, delay, and blur physiological filters were used. The impulse filter was not used because this signal is not captured by our intermittent feedback calculation and participants cannot achieve an above-chance classifier output to reach the target. Targets were randomly and evenly assigned one of the three physiological filters. Unlike the continuous feedback condition, participants were not informed about the different filters because the feedback timing was identical between conditions, although signal quality did vary based on the physiological filter used.

Because we found that accelerating feedback did not significantly affect performance at the task, all trials in the intermittent feedback condition used the 6x acceleration factor, allowing us to record more trials in less time. When calculating the time that participants took to reach targets, we always used the

non-accelerated time (20s per trial), because this is representative of how long the experiment would actually take if it were conducted inside the MRI scanner.

2.4.11 Statistical analysis: cognitive neurofeedback performance

Our outcome measure for performance on each trial was the amount of time needed to find the hidden target. For continuous and intermittent feedback, we constructed separate linear mixed effects models to predict time-to-target using physiological response as a fixed effect and participant as a random effect. Tukey's post-hoc test (α <0.05) was used to determine the differences between each condition. For intermittent feedback, we could not directly measure time-to-target as in the continuous condition because of the feedback acceleration factor. Instead, we calculated this performance metric by counting the number of trials needed to reach the target and multiplying this by 20 seconds (the 'real-time' cost of each trial), and subtracting 5 seconds of time cost because there is no wait period at the beginning of the first trial (3 seconds) and success occurs as soon as the calculated feedback score exceeds the threshold (2 seconds from the final feedback period). To compare continuous and intermittent feedback, we performed two sample t-tests for each physiological response filter, comparing between the continuous and intermittent feedback groups.

2.4.12 Model parameters: automatic learning

We constructed a new 3-way classifier to emulate Shibata et al. (2011) [64], which used three target orientations: 10°, 70°, and 130° (Fig 2.2C). We

used only 3 orientations because our learning model was unable to learn the non-convex objective function associated with the 8-way classifier used in our cognitive experiment. For training our pattern decoder, we simulated 210 training examples (70 of each orientation) with an SNR of 2, using the same V1 model described earlier (tuned to 8 orientations). For our real-time simulation, we also used an SNR of 2 (σ_n=0.5). Unlike our cognitive simulation, where spontaneous activity corrupted the feedback signal and was treated as noise, here we leveraged this 'noise' whenever it spontaneously matched the desired pattern of activity. Therefore, we did not have to increase the SNR as we did in the cognitive experiment in order to make the signal learnable. Also unlike our cognitive experiment, we did not apply a tuning curve to the classifier outputs because we wanted to match the feedback signal presented by Shibata et al. (2011) [64].

2.4.13 Procedure: automatic learning simulation

We simulated five hours of neurofeedback training per simulated participant with a learning rate of 1% per 20 seconds, roughly matching the time scale of learning found by Shibata et al. (2011) [64]. For intermittent feedback simulations, this corresponded to a rate of 1% per trial; for continuous simulations, this corresponded to a rate of 0.1% per 2 second TR.

All four physiological filters from the cognitive experiment (Fig 2.1E) were used in the automatic simulation. We also had five possibilities for internal models (Fig 2.5A). For continuous feedback trials (Fig 2.5B), we used the four phys-

iological filters for our four possible internal models: each matched filter should capture the time series of neural activity that resulted in the continuous feedback signal. For example, if the true physiological filter is an HRF, an internal model of HRF would apply the feedback to a memory trace of the preceding neural activity that gave rise to the feedback signal (Fig 2.5D). For intermittent feedback trials (Fig 2.5C), we used a single internal model generated by the cue-wait-feedback trial structure: activity during the 6-sec cue period is kept in memory and reinforced each trial based on the change in the delayed feedback signal. The cue structure also ensured that conditioned activity was only elicited during the cue period (Fig 2.5E). The intermittent feedback signal was calculated using an average of the recorded response during the wait period, similar to cognitive intermittent trials. Therefore, there were 20 total conditions simulated: 16 for continuous feedback with four physiological filters and four possible internal models, and 4 for intermittent feedback with only one internal model (cue). Because the simulated time series was non-deterministic due to spontaneous activity, we simulated each condition 1000 times to determine the distribution of responses at each time point over the course of learning.

2.4.14 Statistical analysis: automatic learning

The learning quality for each condition (combination of physiological filter and internal model) was evaluated based on the mean and the 50% confidence interval (CI) of the classifier output at each time point, combined across all simulated participants (1000 per condition). Over the course of 5 hours of simulated

neurofeedback training, simulated participants were categorized into four categories: successful learning, trending learning, no learning, and anti-learning. Successful learning curves had a 50% CI ending well above chance. Trending learning curves increased over time, but at a much slower rate than than successful curves, and had a 50% CI that extended into chance at the end of training. Curves with no learning were flat. Anti-learning curves had a 50% CI that ended below chance. Because these classifications were arbitrary, we further ranked internal models for each physiological filter by the average final value of the classifier at the end of training. Pearson's r was used to assess correlations between conditioned patterns, desired activity patterns, and classifier weight maps. Mean correlations with conditioned patterns were calculated by taking the correlation across 1000 examples and taking the mean of these correlations (e.g. not a single correlation with the mean conditioned pattern).

Chapter 3

A simulation-based approach to improve decoded neurofeedback performance[1]

Abstract

The neural correlates of specific brain functions such as visual orientation tuning and individual finger movements can be revealed using multivoxel pattern analysis (MVPA) of fMRI data. Neurofeedback based on these distributed patterns of brain activity presents a unique ability for precise neuromodulation. Recent applications of this technique, known as decoded neurofeedback, have manipulated fear conditioning, visual perception, confidence judgements and facial preference. However, there has yet to be an empirical justification of the timing and data processing parameters of these experiments. Suboptimal parameter settings could impact the efficacy of neurofeedback learning and contribute to the 'non-responder' effect. The goal of this study was to investigate how design parameters of decoded neurofeedback experiments affect decoding accuracy and neurofeedback performance. Subjects participated in

[1]This chapter, in full, was published as an article entitled "A simulation-based approach to improve decoded neurofeedback performance" published in NeuroImage 2019. Oblak, Ethan F.; Sulzer, James S.; Lewis-Peacock, Jarrod A., Elsevier, 2019. The dissertation author was the primary author of the manuscript. The author was responsible for conceptualization and design of the experiment, fMRI data collection, analysis, and visualization of this research.

three fMRI sessions: two 'finger localizer' sessions to identify the fMRI patterns associated with each of the four fingers of the right hand, and one 'finger finding' neurofeedback session to assess neurofeedback performance. Using only the localizer data, we show that real-time decoding can be degraded by poor experiment timing or ROI selection. To set key parameters for the neurofeedback session, we used offline simulations of decoded neurofeedback using data from the localizer sessions to predict neurofeedback performance. We show that these predictions align with real neurofeedback performance at the group level and can also explain individual differences in neurofeedback success. Overall, this work demonstrates the usefulness of offline simulation to improve the success of real-time decoded neurofeedback experiments.

3.1 Introduction

Multi-voxel pattern analysis (MVPA) extracts information about a person's cognitive state by analyzing spatially distributed patterns of functional MRI activity [49, 30]. This approach has become ubiquitous in cognitive neuroscience since the seminal work of Haxby et al. (2001) [31] identified distributed and overlapping representations of visual object categories in temporal cortex. MVPA is especially useful for isolating fine-grained relationships between brain activity and behavior, such as orientation tuning [38, 33] and complex motor programs [79, 44] which are inaccessible to other human neuroimaging analysis methods. However, despite the increased signal-detection sensitivity of MVPA, conventional neuroimaging research is limited in its ability to draw causal infer-

ences about brain-behavior relationships.

Investigation into causal mechanisms of MVPA representations of neural activity requires this activity to be modulated. However, techniques such as TMS [75] and tDCS [9] are incapable of modulating fine-grained patterns of neural activity. Operant conditioning of neural activity, known as neurofeedback, uniquely enables self-modulation of a target neural circuit through feedback, most often presented visually [67, 65]. Early work in fMRI neurofeedback mirrored contemporary univariate techniques in offline fMRI analysis [58]. In recent years, MVPA-based neurofeedback techniques have taken hold [47]. For instance, a seminal work by Shibata et al. (2011) [64] used neurofeedback based on decoded activity from early visual cortex, a process dubbed 'decoded neurofeedback' or 'DecNef'. The researchers were able to show that individuals could learn to self-modulate a targeted pattern of brain activity related to a given orientation of a visual grating without stimulus presentation. Intriguingly this was associated with heightened perceptual acuity specific to the underlying stimulus. Thus, used in this manner, decoded neurofeedback is a powerful and unique tool in neuroscience that can manipulate neural activity patterns to reveal causal relationships with behavior. In addition to further studies investigating low-level visual perception [3], this technique has been used in more translational applications including fear conditioning [41], fear reduction [70], confidence judgements [12], and facial preference [63].

It is well-known that a large proportion (up to 30%) of willing participants are unable to self-regulate their brain activity through neurofeedback training

[2, 28]. The causes of this are not well understood, and the 'non-responder' problem remains a key challenge for neurofeedback research and clinical translation. While the non-responder effect is described as a participant's inability to control a reliable feedback signal, we suggest that the reliability of the feedback signal itself is a larger problem. Indeed, our previous work showed how properties of the feedback signal can significantly affect decoded neurofeedback performance using a novel simulation paradigm [53]. Using feedback based on simulated brain activity in visual cortex, participants performed simple 'cognitive strategies' by choosing how to rotate an oriented grating clockwise or counterclockwise until a hidden target orientation was found. This simulation paradigm enabled the manipulation of 'neurofeedback' provided to the participant to reflect the signal quality and timing of realistic neural activity, and of unrealistic neural activity that would be impossible to present in the scanner by altering or removing the hemodynamic delay. Therefore we could link explicit strategy choices, and thus neurofeedback performance, with the characteristics of the feedback signal received. The approach produced insights into how fMRI neurofeedback presentation can enhance or inhibit learning; for example, intermittent feedback is better than continuously presented feedback when participants have a poor understanding of the hemodynamic properties of the brain signal. However, these simulations did not account for a key element in neurofeedback performance as it relates to decoded neurofeedback: the accuracy of decoding the desired fMRI activity patterns in real-time.

Decoding accuracy can vary widely between experiments and condi-

tions. Standard processing techniques, such as normalization, detrending and averaging over time will all affect decoding accuracy [29]. However, to date there has been no systematic approach to investigating the effects of these parameters on neurofeedback performance. Numerous decoded neurofeedback studies lack an empirical justification for parameter selection [76], leaving the possibility of suboptimal neurofeedback training, which may contribute to the non-responder problem. The goal of the present study was to examine how real-time fMRI decoding accuracy is affected by these parameters, and likewise, how decoder accuracy contributes to neurofeedback performance.

Being able to address this question in a systematic manner requires explicit knowledge of neurofeedback strategies being used by participants. However, cognitive strategies used for neurofeedback, which commonly take the form of mental imagery [17], can be difficult to identify and quantify. Here, we simplified this challenge by focusing on a restricted set of explicit strategies: individual finger movements, which are supported by neural correlates in primary sensorimotor cortex (M1/S1). There is ample literature on fMRI neurofeedback of mean regional activity in M1/S1 [88, 77, 11, 23], and evidence that univariate M1/S1 self-modulation is associated with improvements in fine-motor control. For instance, Bray et al. (2007) [8] found improved reaction time following M1/S1 neurofeedback training, and Blefari et al. (2015) [6] observed a positive correlation between precision grip motor skill and neurofeedback performance. There are, however, no published attempts at decoded neurofeedback for M1/S1. Thus, by using a well-defined neural circuit (M1/S1) and measurable

strategies (finger pressing), we sought to gain insight more generally into how people learn to use decoded neurofeedback, and under what conditions such learning is best facilitated.

Here, we designed a 'finger localizer' experiment based on previous finger individuation decoding experiments (e.g. Diedrichsen et al. 2012, Ejaz et al. 2015 [18, 19]) that could be used to train fMRI pattern classifiers for a neurofeedback experiment (Fig 3.1). We had participants (N=6) complete two of these localizer sessions, on separate days, which allowed us to investigate multiple parameters that impact real-time decoding performance in M1/S1. We first simulated participant neurofeedback performance using feedback yoked to individual localizer trials. This fully automated simulation helped us examine estimated neurofeedback performance in different conditions such as changes in region-of-interest (ROI) and different feedback success thresholds. Then, we recruited a new set of human participants (N=10) to perform this target-finding experiment with the same yoked neurofeedback and compared performance to participants in a real neurofeedback session. The combined simulation and experimentation provide a unique method for investigating fundamental questions about neurofeedback. The results may help to mitigate the non-responder problem, making decoded neurofeedback a more robust procedure.

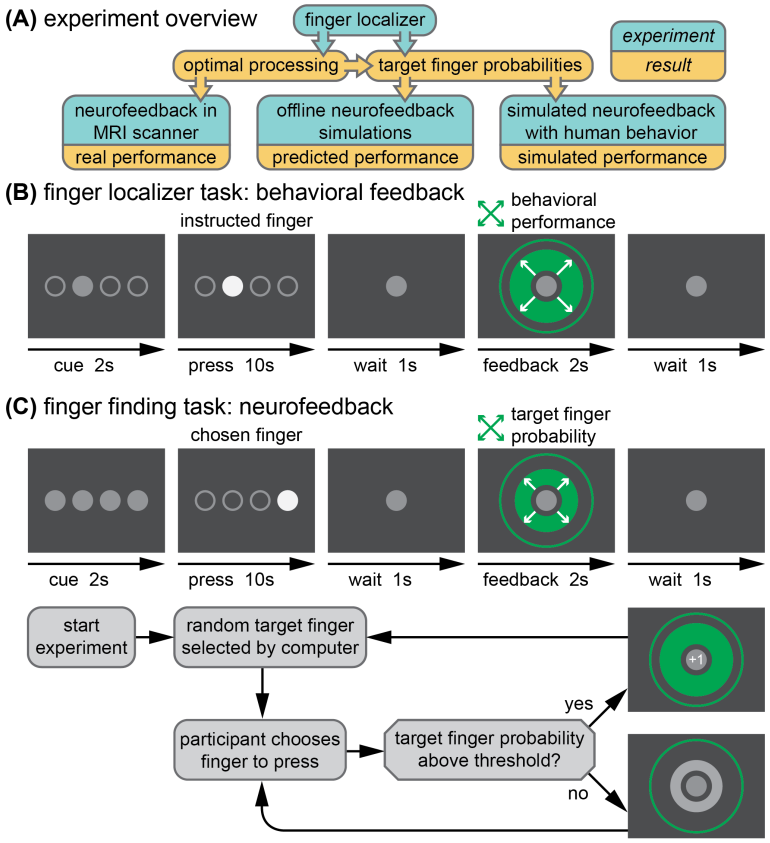

Figure 3.1: **Experimental design. (A)** A finger localizer experiment was used to identify optimal processing parameters for real neurofeedback and to generate finger probabilities for use in simulated neurofeedback experiments. In both localizer **(B)** and neurofeedback **(C)** trials, a cue precedes a 10 sec period of finger pressing at 1 Hz, followed by feedback. The localizer feedback reflects behavioral performance for repeated presses of a finger chosen by the experimenter. The neurofeedback reflects the real-time fMRI decoder output for the target finger based on presses of a finger chosen by the participant. Below, the decision process for advancing trials in the neurofeedback session is presented. The target finger remains the same from trial to trial until a predetermined success threshold is reached, at which point a new random target finger is selected.

3.2 Materials and methods

3.2.1 Participants

Six healthy participants (2 female, average age 26.4 years, SD=2.4) were recruited from the University of Texas at Austin community in accordance with the University of Texas Institutional Review Board. This sample size is in accordance with other individual finger mapping tasks [19]. All subjects completed two localizer sessions, but one subject was unable to participate in the neurofeedback session due to a hand injury that occurred after the second localizer session. An additional ten healthy participants (3 female, average age 24.3, SD=3.6) were recruited for a simulated neurofeedback experiment using the brain data from the localizer sessions of the original group of participants. Written informed consent was obtained from all participants.

3.2.2 General procedure

The experiment consisted of three fMRI sessions separated by at least 24 hours: two localizer sessions followed by one neurofeedback session. The localizer and neurofeedback sessions were similar in structure, as shown in Fig 3.1. The primary purpose of two localizer sessions was to identify the fMRI activity patterns in sensorimotor cortex corresponding to pressing each of the four fingers of the right hand (index, middle, ring, little). However, the secondary purpose of the localizer was to imitate the timing and processing limitations of a real-time fMRI neurofeedback session. Therefore, the duration of trials and runs were identical in both types of sessions, with both consisting of 8 fMRI

runs. These finger-specific activity patterns identified in the localizer were used as targets in the neurofeedback session.

Each run began with a 40 sec baseline period, in which only a grey fixation circle was visible (diameter: 1.5° of visual angle). During the final 3 sec of the baseline period, the fixation circle flashed white at 1Hz to indicate the beginning of trials. Each run consisted of 20 trials of 16 sec each: 2 sec to cue the target finger, 10 sec of finger presses, 1 sec of rest, 2 sec of feedback, and 1 sec of rest before the next trial. On each trial, four circles appeared in the center of the screen (corresponding to the four fingers; 1.5° each, spanning 10° horizontally total) and were used to coordinate finger presses. In the cue period of the localizer task, only one circle turned grey indicating that this was the finger to be pressed on the trial. In the neurofeedback task, all circles turned grey indicating that the participant should choose one finger to press for the duration of that trial. Then, finger presses were cued at a rate of 1Hz for 10 sec with a filled white circle corresponding to the cued (localizer) or selected (neurofeedback) finger.

To ensure consistent behavior from participants, we encouraged rhythmic presses. Participants received positive visual feedback if presses occurred within a specific response window (200-500 ms) of each 1-sec epoch during the 10-sec pressing period. This response window was dynamically adjusted during the localizer sessions (see Section 3.2.3 for details), but remained constant for the neurofeedback session. The cued (or chosen) finger was filled in with a color corresponding to a participant's performance on that press, beginning

when the finger was pressed and ending at 800 ms into the 1-sec press epoch. Presses that occurred inside the response window filled the pressed finger's circle green, and presses that were either too fast or too slow filled the circle yellow. If the incorrect (or unchosen) finger was pressed, the correct finger's circle filled red. After a brief 1-sec wait period, trial-ending visual feedback appeared as a centrally presented green circle (2-10°) that expanded or contracted based on performance during the preceding 10-sec pressing period. In the localizer session, feedback was based on the rhythmicity of presses on that trial (i.e., the proportion of presses made within the desired response window). In the neurofeedback session, feedback was based on the correspondence between the pattern of fMRI activity for the target finger learned by the classifier during the localizer sessions, and the actual real-time pattern of fMRI activity evoked by the chosen finger on that trial. On the first trial, the feedback circle expanded smoothly from the origin to a diameter corresponding to the feedback value. At each subsequent trial, the feedback circle expanded or contracted over 500ms from the previous diameter to the updated diameter to ensure a smooth visual display. When the feedback on a neurofeedback trial exceeded the 'target found' success threshold, the starting point for feedback on the next trial was reset to zero and a new target was selected (see Section 3.2.4 and Fig 3.1C).

3.2.3 Localizer sessions (Days 1 and 2)

As stated earlier, the purpose of localizer sessions was to identify the fMRI activity patterns in sensorimotor cortex corresponding to pressing each of

the four fingers of the right hand (index, middle, ring, little). The general task procedures for the localizer task are described above. All participants completed two localizer sessions separated by no more than 7 days (5+/-2 days, mean+/-s.d.). In each session, the 8 fMRI runs consisted of 20 total trials, with 5 trials for each of the 4 fingers. The order of trials was pseudorandomized to ensure an approximately equal number of each finger transitions (including pressing the same finger two trials in a row). Both localizer sessions were identical other than the order of button presses. As described above, we encouraged rhythmic presses by providing visual feedback (color-filled circles) for each finger press based on whether it was made within a desired response window (200-500 ms). In the localizer task, one 'point' was awarded for each correct response made within this window. Points were tallied at the end of each trial and mapped onto the green feedback circle, with 0 points corresponding to the minimum circle diameter and 10 points corresponding to the maximum diameter. The total score was also tallied and presented to participants at the end of each run. To control for task difficulty, an adaptive staircase procedure was used to incrementally adjust the rewarded response-time window based on performance after each trial. A threshold of 70% correct responses (7 points) was selected for staircasing. If this threshold was exceeded (8 or more points), then the upper limit of the time window decreased by 20 ms (i.e., to 480ms), making the task slightly harder. If performance was below this threshold (6 or fewer points), then the upper limit of the window increased by 20 ms (i.e., to 520ms), making the task slightly easier. If performance matched this threshold, no changes were made to the response

window.

Participants were instructed to gain as many points as possible by pressing the cued finger during the correct response window, and that the size of the circle at the end of each trial would represent the proportion of presses within that response window. Participants were allowed to perform a small number of trials (10) to understand the approximate response window before performing the task inside the scanner.

3.2.4 Neurofeedback session (Day 3)

The purpose of the neurofeedback session was to investigate whether human participants could efficiently and accurately interpret fMRI decoder outputs related to pressing the four fingers of the right hand on a trial-by-trial basis. As such, the participant's goal was to respond to the decoded neurofeedback by finding and then pressing with the finger associated with the targeted brain pattern (i.e. 'target finger'). Participants had 160 trials (20 trials per run, 8 runs total) to find as many target fingers as possible. A series of target fingers was pseudo-randomly generated for the experiment. A full set of 160 targets was generated in the unlikely case that a target was found each trial. The order of targets was determined by a concatenation of 20 lists that each contained a randomly shuffled arrangement of 8 finger targets (2 for each finger). This allowed for the target finger to occasionally repeat and to prevent prediction of the target finger (e.g. by process of elimination over a series of targets). Participants chose one finger to press each trial. After 10 presses of the same finger,

the feedback circle appeared, as in the localizer sessions, except that here the size of the circle corresponded to the fMRI decoder output for the target finger in sensorimotor cortex (M1+S1, see Section 3.2.7). The decoder outputs (from 0 to 1, for each finger) indicated the likelihood estimates from the fMRI pattern classifier that the fingers were pressed. The minimum diameter of the feedback circle corresponded to 0% probability of the target finger, and the maximum diameter corresponded to 100% probability (Fig 3.1C). If the participant had been pressing the target finger during the trial, its output value should be relatively high. Note that the target output could also be spuriously high when a different finger is pressed if the data on that trial is particularly noisy or the decoder performs poorly in general. If the output exceeded a chosen threshold (50% probability), the feedback circle turned green and a '+1' text appeared in the fixation circle, indicating that a target had been reached and a new random target would be selected. If the decoder output for the target finger was below the chosen threshold, the feedback circle appeared grey and the target remained for the next trial. The total score (number of targets reached) was tallied and presented to participants at the end of each run. If the current target was not reached by the end of a run, that target was continued at the beginning of the next run.

Participants were informed of the experimental paradigm: that a random target finger would be selected, and that they had to choose a finger to press rather than being cued to a specific one. If the computer calculated that their selection was correct, the circle would be large and green with a '+1' and a

new random target finger would be selected. If the computer calculated that their selection was incorrect, the circle would be smaller and grey and the same target finger would remain. Participants were instructed to find as many targets as possible to maximize their score. They were also told that the computer was making decisions based on their real-time brain activity, which may not always be accurate, and thus they may need to guess the same finger again even if the circle was grey when they previously selected it. They were informed that the relative size of the circle represented the confidence of the computer. Participants were allowed to perform a small number of trials (10) of the task outside of the scanner using simulated neurofeedback (see Section 3.2.11 for details) to confirm that they understood the task.

3.2.5 Apparatus

Finger presses were recorded from the index, middle, ring, and little fingers of the right hand using a four-button box (Current Designs, Philadelphia, PA). The button box was affixed to a wooden board, which lay on the participant's lap. Sandbags were placed under the right arm according to participant comfort in the first localizer session, and placed in the same position during the second and third sessions. Participants received visual instructions and visual feedback through a back-projection screen, driven by Python and PsychoPy [55] running on a MacBook Pro.

3.2.6 fMRI acquisition

Participants were scanned in a Siemens Skyra 3T scanner with a 32-channel head coil. For all fMRI sessions, the same EPI sequence was used (TR=2 sec; 36 slices; in-plane resolution 2.3x2.3 mm; 100x100 matrix size; 2.15 mm slice thickness; 0.15 mm slice gap; 2x multiband factor). Each fMRI run consisted of 180 volumes (TRs), with 3 dummy TRs acquired before each run to allow for steady-state magnetization. After auto-alignment to the AC-PC plane, a manual adjustment was performed to ensure full coverage of the motor cortex. The same manual adjustment parameters were applied to the subsequent localizer and neurofeedback sessions. A high-resolution T1-weighted anatomical image (MEMPRAGE; FoV 256 mm (256 x 256 matrix), 176 sagittal slices; in-plane resolution 1x1mm; 256x256 matrix size; 1 mm slice thickness; TR=2530 ms; TE=1.64/3.5/5.36/7.22) was also acquired during the first localizer session. To collect real-time fMRI data, a high-performance GPU was installed in the Measurement And Reconstruction System (MARS) that handles image reconstruction; this dedicated hardware speeds reconstruction times by more than a factor of ten. From there, the raw images are immediately sent via a 10Gb/s fiber link that runs directly from the MARS to the analysis workstation (a Dell Precision T7600n, with dual eight-core E5-2665 2.4GHz processors, 64GB 1600MHz registered ECC memory). Data is then transformed into a standard NIFTI imaging file format for preprocessing, registration, and MVPA analysis using custom Python software (Instabrain; https://github.com/LewisPeacockLab/instabrain).

3.2.7 Regions-of-Interest

Regions-of-Interest (ROIs) within sensorimotor cortex were identified using a Freesurfer [14] segmentation of the high-resolution MEMPRAGE image. Four regions were used as the basis for ROI analysis: Brodmann areas 4a, 4p, 3a, and 3b. All masks were generated simultaneously in each participant's functional space using Freesurfer's mri_label2vol to ensure that each functional voxel was assigned to only one of the regions. These masks were then combined into the left primary motor cortex (M1: combined BA4a and BA4p) and left primary somatosensory area (S1: combined BA3a and BA3b). Five additional ROIs were then generated from combinations of these two primary ROIs: a combined ROI (M1+S1), and reduced-overlap versions ($^{-}$ and $^{--}$) of M1 and S1. To create these versions, the adjacent ROI (for M1: S1; for S1: M1) was expanded by one or two voxel widths ($^{-}$: 2.3mm, $^{--}$: 4.6mm, using fslmaths options: e.g. -kernel sphere 2.3 -dilM) and subtracted from the standard ROI.

3.2.8 fMRI processing

3.2.8.1 Rigid body motion correction

The mean of the first fMRI run of the first localizer session was used as a reference functional image (RFI). All functional volumes from both localizer sessions underwent rigid body motion correction to the RFI template using FSL's MCFLIRT. Each functional voxel then underwent some combination of detrending and normalization (z-scoring) on a run-by-run basis.

3.2.8.2 Detrending (high pass filtering)

Three levels of first-order (linear) detrending were investigated: none, real-time (using all prior data from the current run to linearly detrend up to the current time point), and offline (using data from the entire run to linearly detrend). Higher order (polynomial) detrending or other forms of high-pass filtering were not considered in this analysis. For all analyses in which other factors were varied (decoding timing, z-scoring, ROIs), real-time detrending was used.

3.2.8.3 Z-scoring (normalization)

Four types of z-scoring were investigated: none, baseline rest (using the baseline rest period at the beginning of each run), real-time (using all prior data from the current run), and offline (using data from the entire run). The baseline rest detrending condition was further subdivided to evaluate the impact of the amount of baseline data used, from 2 TRs (4 sec) up to 20 TRs (40 sec). This baseline period began with the first 'real' TR of each run, following the 3 dummy TRs collected at the beginning of each run, ensuring that transient magnetization artifacts did not affect the baseline estimate. For all analyses in which other factors were varied (decoding timing, detrending, ROIs), baseline z-scoring from the entire 40 sec baseline period was used.

3.2.8.4 Feature extraction and decoding

In each localizer run there were 40 trials per finger, thus 80 total trials of data were collected per finger. Mean voxel activities were extracted for each trial

using a 3-TR (6-sec) sliding window across the trial. Resulting fMRI activity patterns were then masked by ROIs and submitted to a sparse multinomial logistic regression classifier (SMLR; Krishnapuram et a. (2005) [46]). For within-session analyses, a leave-one-run-out cross-validation was performed to determine decoder accuracy. For across-session analysis, the decoder was trained on one localizer session and applied to the other localizer session (and vice versa).

3.2.8.5 Classifier importance maps

Classifier importance maps [50] were calculated to identify voxels that contributed significantly to the identification of each finger. For each finger, 'importance' values at each voxel were calculated by multiplying the voxel's decoder weight for that finger by its mean activity level during that finger's press. Positive importance values resulting from positive decoder weights were considered positive, whereas positive importance values resulting from negative decoder weights were considered negative; negative importance values were ignored, as performed by McDuff et al. (2009) [50]. An overall 'winner-takes-all' representation was further created by taking the maximum absolute value of importance at each voxel across all 4 fingers. Representations were then projected onto the cortical surface using Freesurfer [14] and visualized using PyCortex [25].

3.2.8.6 Chosen parameters for neurofeedback session

For the neurofeedback session, real-time detrending was selected, and z-scoring was based on the full 40-sec baseline rest period. FSL's MCFLIRT was used to realign real-time functional volumes to the RFI template for each participant. Based on offline analyses of the localizer data, we sought to maximize the quality of decoded neurofeedback by focusing on fMRI data from the combined M1+S1 ROI during the final 6-sec time window prior to feedback (TRs 4-6) on each trial.

3.2.9 Overview of neurofeedback simulations

Our method to develop neurofeedback simulations is outlined in Fig 3.1A. Once the optimal parameters for decoding were chosen (Section 3.2.8.6), we used these parameters to calculate across-session fMRI decoder outputs from every trial in every localizer session (160 trials x 2 sessions x 6 participants = 1,920 trials, with 480 trials per finger). These decoder outputs were used to calculate target finger probabilities in either a fully offline simulation (Section 3.2.10 or a simulated neurofeedback experiment with human participants (Section 3.2.11).

3.2.10 Predicted performance with offline simulations of neurofeedback

To help calibrate design parameters and predict human performance in the neurofeedback session, we performed an offline simulation using fMRI data from the localizer sessions as described in Section 3.2.9. As in the real neu-

rofeedback session, a pseudo-random target finger was chosen for every trial. A simple search strategy was chosen for the behavioral simulation: choosing each of the fingers sequentially, starting with the index, until the target was found (i.e., *index, middle, ring, little, index-...*). For each simulated pressing trial, a sample trial corresponding to the selected finger was randomly chosen (with replacement) from the full set of localizer trials to simulate the brain activity on the trial. If the decoder output for the target finger exceeded a success threshold (which could occur due to noise, leading to a false positive) then the target was considered found and a new target was chosen for the next simulated trial. Several conditions were tested: two different ROIs (M1+S1, and M1 alone), and a range of success thresholds (from 25% to 90% in 5% increments). For each combination of conditions, a total of N=1,000 participants were simulated, each performing 160 trials of simulated neurofeedback, as in the real experiment.

3.2.11 Simulated neurofeedback with human behavior

We also conducted a behavioral experiment to compare neurofeedback performance using human strategies compared to the simulated (sequential) behavioral strategy. Using the same across-session decoder outputs as in the offline simulations of neurofeedback, a set of human participants (N=10) attempted to find targets as in the real neurofeedback experiment. The structure of the experiment was similar to the neurofeedback session except accelerated in time: participants only had to make a single press (rather than 10-sec of presses) to choose their finger, and feedback appeared immediately after the

press. This accelerated timing allowed us to investigate two ROIs (using decoded neurofeedback from M1+S1 and also from M1 only) in a short period of time. We previously found no difference in trials-to-target for accelerated simulated feedback compared to the significantly slower feedback pace of real-time fMRI [53]. Furthermore, participants had no knowledge of the true target: only a one-dimensional feedback signal was provided for the target, which meant that false positives were possible, mimicking a true neurofeedback experiment in which incorrect strategies may spuriously cause positive feedback signals. We conducted 8 consecutive runs of trials for each ROI (20 trials per run, ROI order randomized across participants), similar to the real neurofeedback experiment. This experiment lasted approximately 10 minutes per participant.

3.2.12 Statistics

A separate linear mixed-effects model (nlme in R [56]) was created to predict decoder accuracy for each of real-time decoding, baseline sensitivity, normalization, and detrending analyses. Each model included ROI (S1 or M1) and decoding type (within or between session) as fixed effects and subject as a random effect. Tukey's post-hoc test (α <0.05) was used to determine the differences between each condition. To compare decoding accuracy across ROIs (M1+S1, M1, S1, $M1^{-}$, $S1^{-}$, $M1^{--}$, and $S1^{--}$), paired t-tests (df=5) were used. To compare the correlation of decoder outputs across ROIs, the mean correlation (averaged across both localizer sessions) for each subject was Fisher Z-transformed and submitted to a paired t-test. Performance of real neuro-

feedback and simulated neurofeedback participants were compared using an independent groups t-test (df=13).

3.3 Results

3.3.1 Real-time decoding limitations

Using fMRI data from the two localizer sessions, we characterized the limitations of decoding individual finger presses in real-time from fMRI activity in M1 and S1 by manipulating key analysis parameters: timing, baseline duration, normalization type, and detrending type (Fig 3.2).

3.3.1.1 Real-time decoding over time

The timing limitations of real-time decoding were related to the intermittent feedback timing. In order to deliver feedback at the scheduled time (11 sec after the beginning of each pressing period), we could only use data gathered up to 1 sec before the feedback period. However, the timing of this feedback period could be adjusted to save time or optimize decodability. To assess the optimality of feedback timing, we analyzed decoding accuracies at TRs 5, 6, and 7, corresponding to our hypothesized optimal feedback TR (6) and the TRs immediately before and after (5 and 7). We found decoding at TR 6 to be significantly better than TR 5 (+5.6% decoding, Tukey's HSD, $p<0.001$), whereas TR 7 was not significantly different than TR 6 (-0.1% decoding, p=0.996). Fig 2A illustrates these differences. This analysis also revealed a large main effect of ROI (S1 $>$ M1: +20.1% decoding, $p<0.001$) and a small but reliable main effect

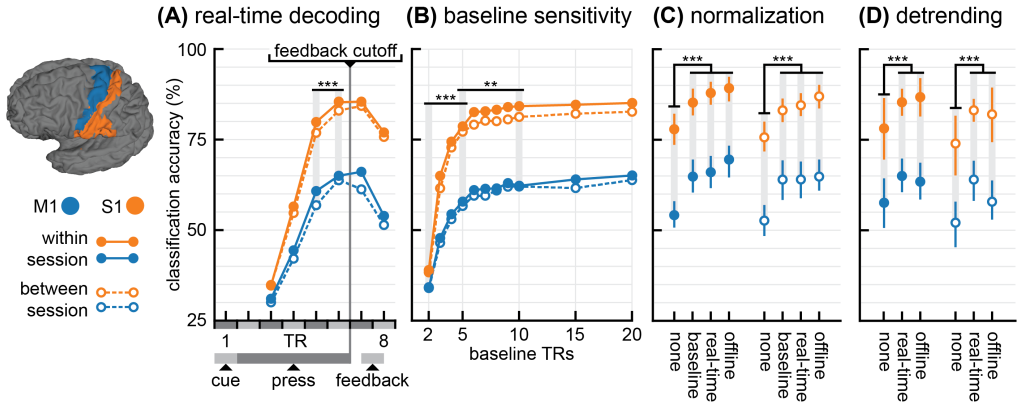

Figure 3.2: **Real-time decoding limitations.** **(A)** Real-time finger decoding over time (chance: 25%). The feedback cutoff (1-sec before the feedback period) is the last time at which fMRI data can be used for neurofeedback. Each displayed time point includes time-averaged fMRI data from the current time repetition (TR) and the two previous TRs; real-time detrending and baseline (20 TRs) z-scoring were used. **(B)** Sensitivity of decoding to the baseline time period used for normalization (z-scoring); real-time detrending was used. **(C)** Decodability for four different types of normalization: none, z-scoring based on 20 TRs of baseline data, realtime z-scoring, and z-scoring based on a full run of data, which is equivalent to offline analysis; real-time detrending was used. **(D)** Decodability for three different types of detrending: none, real-time detrending, and offline detrending based on a full run of data; baseline (20 TRs) z-scoring was used. Error bars indicate a 95% confidence interval. M1 shown in blue and S1 shown in orange. Within session decoding shown with solid lines and closed circles and between-session decoding shown with dashed lines and open circles. Selected statistical comparisons shown. Stars indicate significant differences at $p<0.01$ (**) and $p<0.001$ (***). Error bars omitted in (A) and (B) for clarity; see (C) and (D) for typical error bars.

of session (between session $<$ within session: -2.8% decoding, p=0.004).

3.3.1.2 Baseline sensitivity

We next investigated how sensitive the decoder was to different amounts of baseline data used for normalization (z-scoring). We analyzed four amounts of baseline data: the first 2 TRs, 5 TRs, 10 TRs, and 20 TRs of the run (Fig 3.2B). Increasing from using 2 to 5 TRs for baseline normalization significantly increased decodability (+31.6% decoding, $p<0.001$). Increasing from 5 to 10 TRs also significantly increased decodability, but with diminishing returns (+4.8% decoding, $p<0.001$). There was no significant difference in decodability between 10 and 20 TRs (+1.9% decoding, p=0.58).

3.3.1.3 Normalization

Next, we analyzed how different types of normalization (z-scoring) affected decoding. We first compared baseline z-scoring (using the full 20-TR baseline period), real-time z-scoring (using all previous data from the run), and offline z-scoring (using all the data in the run, Fig 3.2C). Each of these was significantly better than performing no z-scoring at all ($p<0.001$), yielding mean decoding increases of 9.2%, 10.5%, and 12.4% decoding for baseline, real-time, and offline conditions, respectively. Within these three types of normalization, there was only a significant difference when comparing baseline to offline z-scoring (-3.3% decoding, p=0.022).

3.3.1.4 Detrending

Finally, we investigated the effect of different types of detrending on decoding. Both real-time and offline detrending were significantly better than no detrending ($p<0.001$), with a mean decoding increase of 8.9% for real-time detrending and 7.2% for offline detrending (Fig 3.2D). There was no significant difference between real-time and offline detrending (p=0.45).

3.3.2 Decoding and information shared across ROIs

We next investigated decoding and decoder outputs in different ROIs (Fig 3.3A) based on the same localizer data, to investigate if motor and sensory representations could be separated without significantly affecting decodability.

3.3.2.1 Decoding accuracy

Across-session decoding accuracy was highest in the combined M1+S1 region (83.4%) and in the isolated S1 region (83.3%), with no significant difference between the two (p=0.85). M1+S1 had significantly better decoding than M1 (+18.2% decoding; p=0.002). Moving to the reduced $M1^{-}$ from M1 was significantly worse (-13.8%, p=0.019), and also to $M1^{--}$ from $M1^{-}$ (-8.2%, p=0.027). $S1^{-}$ was not significantly worse than S1 (-5.94%, p=0.073), but $S1^{--}$ was significantly worse than $S1^{-}$ (-26.7%, $p<0.001$). Fig 3.3B illustrates differences in decoding accuracy. By attempting to isolate primary somatosensory and motor cortices, decoding accuracy was significantly impaired.

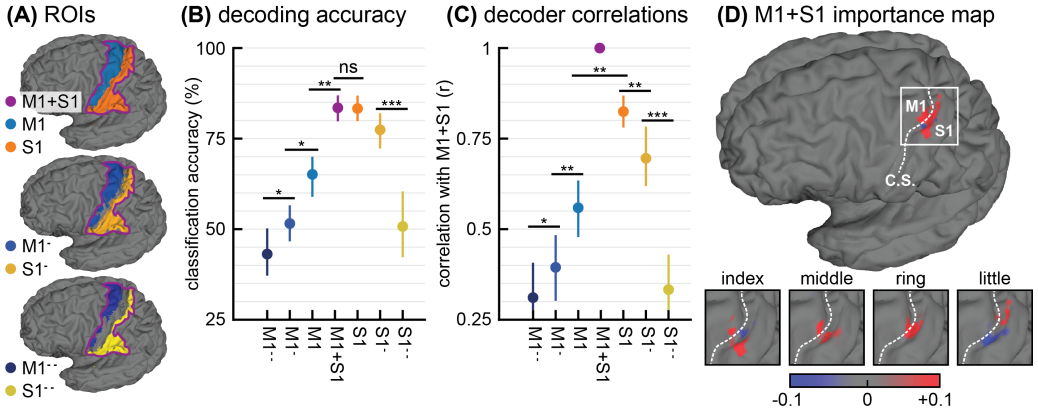

Figure 3.3: **Decoding and information transfer across ROIs. (A)** ROIs used for analysis. **(B)** Between session decoding for ROIs. **(C)** Correlations between decoder outputs at the same time point but in different ROIs. All correlations are made with the combined M1+S1 decoder outputs, indicating the correspondence of information between the combined M1+S1 decoder and the reduced ROIs. **(D)** Classifier importance maps for the combined M1+S1 decoder of a sample participant, in arbitrary units. C.S. indicates the central sulcus dividing M1 and S1. Cortical visualizations generated with PyCortex [25]. Error bars indicate a 95% confidence interval. Selected statistical comparisons shown. Stars indicate significant differences at $p<0.05$ (*), $p<0.01$ (**), and $p<0.001$ (***). 'NS' indicates no significant differences.

3.3.2.2 Decoder correlations

The decoder outputs from S1 were more strongly correlated with the combined M1+S1 region than were the decoder outputs from M1 correlated to this region (p=0.005). Moving anteriorly, the $M1^{-}$ decoder was more weakly correlated than M1 (p=0.003), and $M1^{--}$ was more weakly correlated than $M1^{-}$ (p=0.016). Similarly, moving posteriorly, the $S1^{-}$ decoder was more weakly correlated than S1 (p=0.003), and $S1^{--}$ more weakly correlated than $S1^{-}$ ($p<0.001$). See Fig 3.3C for correlation results. Despite nearly identical decoding accuracy

between the combined M1+S1 and S1 alone, the information contained by each decoder is not identical; indeed, the combined M1+S1 shares information with both M1 and S1 decoders, albeit weighted more heavily toward S1.

3.3.2.3 Importance maps

Classifier importance maps [50] were generated both for individual fingers (Fig 3.3D, bottom) and as a 'winner-takes-all' map across all fingers (Fig 3.3D, top). The overall map shows that important voxels for finger decoding lie on both sides of the central sulcus, with more on the posterior (S1) side. Furthermore, they tend to be near to the central sulcus, aligning with the observation that motor and somatosensory representations cannot easily be separated. Individual finger maps confirm that the classifier is picking up on localized changes in activity throughout the hand area of sensorimotor cortex rather than overall mean activity changes across the entire region.

3.3.3 Finger finding experiment

3.3.3.1 Predicted performance

We first predicted performance based on a variable success threshold for finding targets in both the combined M1+S1 region and in the M1 region alone (Fig 3.4A). We chose M1 because of its significantly lower decoding accuracy compared to M1+S1, allowing us to investigate how reduced decoding accuracy affects predicted performance.

Across both selected ROIs, increasing the success threshold caused an

exponential increase in the number of trials required to find a target, with diminishing returns on predicted target accuracy. Based on these predictions, a threshold of 50% was selected for subsequent experiments with human participants to maximize accuracy while minimizing the number of trials to target.

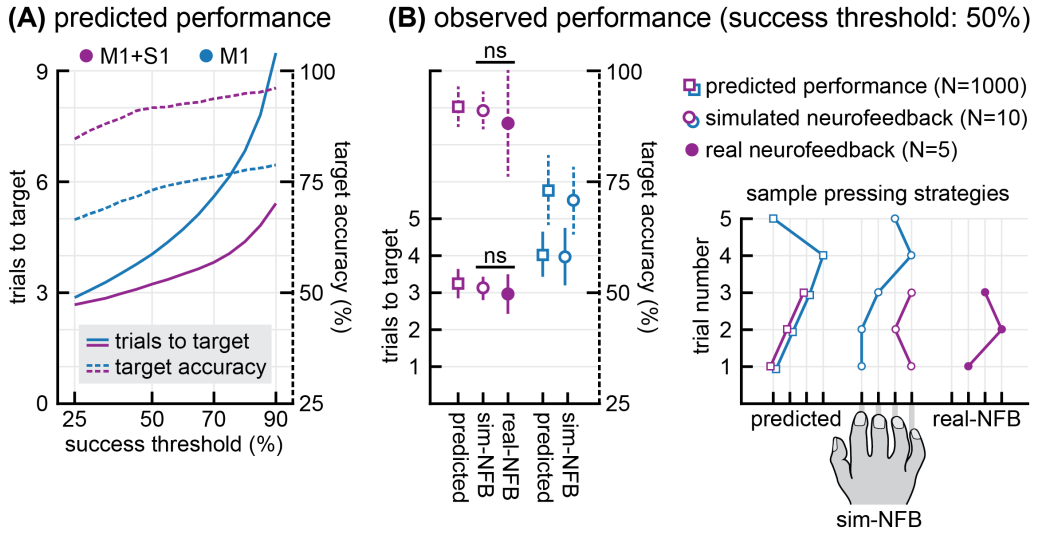

Figure 3.4: **Finger finding neurofeedback experiment performance. (A)** Predicted performance based on between-session decoder outputs from the localizer sessions. The success threshold for finding targets was varied between 25% and 90%. Target accuracy indicates the proportion of targets in which the finger pressed when the decoder output exceeded the success threshold matched the target finger. **(B)** Observed performance for both real neurofeedback and simulated neurofeedback participants using a success threshold of 50%. Trial-by-trial sample pressing strategies are shown for each condition: predicted, simulated, and real neurofeedback. Each tick represents a single finger of the right hand as illustrated. Each line represents one example target search, with the line ending when the decoder output exceeded the target threshold. Due to noise, occasionally the same finger is repeated. Error bars indicate standard deviation. M1 shown in blue and M1+S1 shown in purple. 'NS' indicates no significant differences.

3.3.3.2 Simulated neurofeedback results

We next investigated whether human participants' performance matched our model predictions for the selected success threshold (Fig 3.4B). In M1+S1, we expected 3.23+/-0.29 trials to target (mean+/-s.d.) and 91.7+/-3.7% target accuracy. In our simulated neurofeedback experiment, we recorded 3.12+/-0.12 trials to target with 91.9+/-3.4% accuracy using data from this region. In the M1 region, our predictions were similarly accurate: the prediction was 4.04+/-0.49 trials with 73.1+/-7.1% accuracy, and the simulated neurofeedback result recorded was 3.97+/-0.67 trials with 70.1+/-6.8% accuracy.

3.3.3.3 Real neurofeedback results

We then compared real neurofeedback results to the simulated results in the M1+S1 region that was selected for the neurofeedback experiment (Fig 4B). In the scanner, participants required 2.97+/-0.43 trials to find each target, with 87.7+/-11.7% accuracy. There was no significant difference between this performance and the simulated neurofeedback participants' performance (trials-to-target: $t_{(13)}$=-0.97, p=0.35; accuracy: $t_{(13)}$=-0.78, p=0.45).

Finally, we investigated how decoding accuracy influenced performance on our task (Fig 3.5). We selected the 50% success threshold and M1+S1 region in order to qualitatively compare performances between the three conditions (predicted, simulated neurofeedback, and real neurofeedback). In the predicted dataset, trials-to-target was negatively correlated with decoding accuracy (slope of best-fit line=-4.36, r=-0.41, $p<0.001$ Fig 3.5A) and target accuracy was

positively correlated with decoding accuracy (slope=0.66, r=0.48, $p<0.001$, Fig 3.5B), as expected. The slope for the trials-to-target was negative for simulated neurofeedback (slope=-0.86) and real neurofeedback (slope=-3.19); the slope for decoding accuracy was positive for simulated neurofeedback (slope=0.70) and real neurofeedback (slope=0.93). While decoder accuracy was significantly correlated with our performance metrics in the predicted results, only part of the variance was captured by decoder accuracy (trials-to-target: r^2=16.8%; target accuracy: r^2=23.0%). Because strategies were kept fixed within the predicted results, we suggest that there may always be significant variability in neurofeedback performance that cannot be accounted for by the quality of the decoder or the participant's strategy. Although the effect of decoding accuracy on trials-to-target in the simulated neurofeedback group (-0.86) appears different from the predicted slope (-4.36), the result falls well within the 95% confidence interval (-11.8, 2.89) of repeated samples of N=10 predicted results (1000 bootstrapped samples with replacement).

3.4 Discussion

This study presents a systematic investigation of optimal parameter selection for the design of real-time neurofeedback experiments that rely on multi-voxel pattern analysis of neuroimaging data. We collected fMRI data of participants performing individual finger presses and trained classifiers to discriminate brain activity patterns for each finger in sensorimotor cortex. These classifiers were intended to perform real-time decoding of finger presses in a subsequent

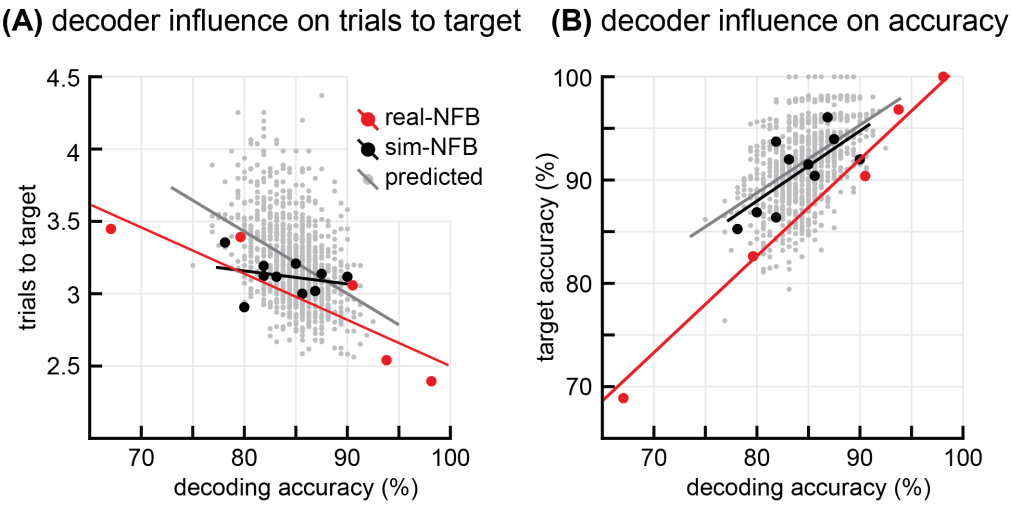

Figure 3.5: **Influence of decoding accuracy on finger finding performance.** **(A)** Correspondence between observed decoding accuracy during the finger finding session and the mean number of trials required to find each target. **(B)** Correspondence between observed decoding accuracy during the finger finding session and target accuracy (proportion of trials in which the decoder output exceeded the success threshold and the pressed finger was also the target finger). Solid lines indicated the best-fit line for each condition.

neurofeedback session. Offline analyses with real-time processing constraints revealed optimal choices for the analysis of these data and the timing of the neurofeedback experiment. Simulated results of neurofeedback performance were confirmed by participants receiving real neurofeedback inside the scanner. This study demonstrates how the offline simulation of neurofeedback performance using real fMRI data can be used to optimize human performance on real-time neurofeedback experiments.

The simulation of neurofeedback performance is a novel approach to the field. While reliance on simulations has long been common in other neu-

roscience subdomains such as visual neuroscience [74], our previous work mentioned earlier [53] was the first instance of simulation in fMRI neurofeedback. Whereas in the aforementioned study, we simulated brain activity based on known parameters of visual cortex activity, here we present recorded brain activity in sensorimotor cortex to both to human participants and to simulated participants with predetermined neurofeedback strategies. A key element to this simulation of neurofeedback is an explicit strategy, i.e. finger pressing, because it can be directly measured and validated both inside and outside of the scanner. Our simulation was validated for explicit strategies through similar outcomes in real and simulated neurofeedback (Fig 3.4B). However, it remains to be answered to what degree the explicit strategies used in this paradigm can represent mental strategies typically used in neurofeedback. Typical decoded neurofeedback experiments rely on implicit learning and do not indicate to participants when they have discovered the 'correct' strategy (as is done in this work using the concept of a 'success threshold'), because the correct strategy is not known by the experimenter. Future work should incorporate more advanced learning models, including implicit strategies, into this simulation paradigm, to determine the extent to which decoding accuracy can predict decoded neurofeedback performance when no explicit strategy is known. We anticipate such simulation of neurofeedback performance to be a valuable tool to improve the efficiency and robustness of experiments, which more recent work in fMRI neurofeedback has begun to explore [16, 61].

Our work shows the benefit of using localizer data to predict neurofeed-

back performance in two ways. First, we were able to design a parameter of our experiment, namely the feedback success threshold of 50%, to optimize predicted neurofeedback performance as a tradeoff between finding successful strategies and finding accurate strategies (Fig 3.4A). These predictions translated to both real neurofeedback participants and human participants interacting with a simulated neurofeedback signal outside of the fMRI scanner (Fig 3.4B). Although our task and model of learning was simple, and the parameter of 'success threshold' was non-standard, this same simulation strategy could be used with a more complex learning model [53, 76] to determine the required duration of an experiment, or to design tuning curves in an adaptive neurofeedback experiment [15]. Second, given our fully designed experiment, we were able to generate a distribution of predicted neurofeedback performance results based on localizer data alone (Fig 3.5). These predicted results show a large variance (especially given that each simulated participant used exactly the same strategy), placing a lower bound on the expected variability across participants given their localizer decoder accuracy. This type of predicted performance distribution could be used as an exclusionary criterion for patients in neurofeedback treatment or to predict the minimum required duration of treatment; it could also be used to alter neurofeedback parameters for individuals based on their own localizer data.

A major goal of this study was to tease apart the non-responder effect by focusing on decoder quality using a task that every participant would be able to figure out. In this way, we ensured that every participant would be a 'responder'

within a short period of time (a few trials). This let us explore how decoder accuracy affects performance without worrying about the participants' strategies. Indeed, the 'finger finding' experiment is not an accurate model when considering the time scale of decoded neurofeedback learning, but we believe that general principles can transfer. For example, a decoder that allows participants to find targets in 3 trials versus 5 trials could equate to a decoder requiring 3 decoded neurofeedback sessions versus 5 decoded neurofeedback sessions to show clear learning.

Our neurofeedback predictions show how a given decoder accuracy translates to neurofeedback performance. In all cases, neurofeedback performance increased with increasing decoder accuracy. Therefore, our secondary goal was to explore which typical parameters of decoded neurofeedback experiments had the largest effect on decoding accuracy. Two standard fMRI preprocessing steps, normalization and detrending, were found to have a large effect on real-time decoding. Real-time z-scoring increased decoding accuracy by 10.5% (Fig 3.2C) and real-time detrending increased decoding accuracy by 8.9% (Fig 3.2D) compared to no preprocessing at all. Critically, these results did not suffer relative to offline decoding, indicating that the real-time preprocessing constraints were not a performance bottleneck.

We next found that we could decode from an earlier timing window than standard decoded neurofeedback experiments without a significant reduction in decoder accuracy. The standard timing window for decoded fMRI neurofeedback is a 6-sec stimulus period followed by a 6 sec decoding period [64],

accounting for the hemodynamic delay. We increased the length of the stimulus period (in this case, finger pressing) to 10 sec, yet decoded 2 sec earlier than Shibata et al. (2011) [64] (Fig 3.2A). For behaviors and ROIs other than those detailed in this work, we recommend designing a localizer with varying stimulus periods and rest periods to determine the best tradeoff between decodability and feedback timing for that experiment

The standard normalization method for decoded neurofeedback is z-scoring using a baseline resting period of 20 sec at the beginning of each fMRI run [64]. Our results support this choice, as there was no significant increase in subsequent decodability when we doubled the length of the baseline period to 40 sec. We also show that real-time z-scoring can be used to achieve similar decoding performance (Fig 3.2B), although this would still necessitate a baseline period at the beginning of each run to ensure reasonable decoding accuracy on the first trial of each run. There may be further confounds associated with real-time z-scoring (e.g. large changes in strategy could skew z-score estimates mid-run), but the data here cannot address these possible confounds.

We observed differences in decoder performance dependent on the specificity and location of the ROI. For instance, we found that by reducing the size of our ROIs by only one voxel width, decoding accuracy was reduced by 14% in M1 and by 6% in S1 (Fig 3.3B). These results are not surprising given the limited spatial resolution of fMRI and high intersubject variability. This evidence suggests that predetermined segregation of ROIs should be handled carefully. If a neurofeedback experiment targets a specific behavior without a well-defined

anatomical hypothesis, then we should err on the side of inclusion and allow the decoder to automatically select relevant voxels in the brain [63]. However, if there is a strict hypothesis based on a neural mechanism in a specific ROI, then it is reasonable to restrict the voxels at the expense of decodability [64]. In our case, we chose a broad M1+S1 ROI because we were not attempting to segregate a specific neural mechanism, such as separating motor output from tactile sensation. If we had a strict motor or sensory hypothesis, isolating the M1 or S1 ROI may be necessary. However, if such segregation was necessary, and subsequently reduced decoder performance, the procedures illustrated here could be used to predict neurofeedback performance, such as the number of trials required to induce neurofeedback learning. Fig 3.5 shows how decoder accuracy is predictive of neurofeedback performance. Thus, one of the contributions of this work is the suggestion that a targeted decoder accuracy should be predetermined together with the goals of the study prior to commencing neurofeedback training.

While here we show the power of simulation of decoded neurofeedback parameters, there are limitations to what we can conclude. By focusing only on M1 and S1, the generalizability of our model to other brain regions is limited. Furthermore, the number of neurofeedback participants was low (N=5), especially compared to the simulated neurofeedback participants (N=10). As expected, we did not find a significant difference in performance between the two groups, tentatively validating our basic model. Running more non-fMRI behavioral participants could show more fine-grained differences between real and

simulated participants, but would require more detailed analysis of participants' strategies, which was not within the scope of this study. Indeed, our previous work [53] had much larger groups (2 groups of N=24 each), but this was due to there being more experimental conditions within each experimental session and a continuous rather than discrete strategy space allowing for more variable strategies between participants. It is also likely that small differences would be found with a larger sample of neurofeedback participants in our simple 'finger finding' task, because participants during this task are receiving feedback from real neural activity and thus have the ability to modulate the feedback signal beyond the simple choice of which finger to press. While participants were not explicitly instructed to self-modulate their brain activity, they were informed that feedback was coming from their own brain. Thus, they may learn to maximize the decoder output for the pressed finger, for example by pressing harder or more individually with each finger, which would increase performance at the 'finger finding' task. Alternatively, they may learn to press *less* individually, which may have a larger chance of randomly triggering the target finger decoder output even if they are pressing the non-target finger; this neurofeedback strategy would lead to a decrease in performance at the 'finger finding' task. Critically, the experimental setup for this work used a simple button box and did not record forces exerted by each finger, and thus we could not include these factors in our model. Future work will aim to measure these factors: if differences are found, the model could be improved to address these more subtle facets of the experiment. This would help us determine the composition of variability in de-

coder output: in the current work, we cannot conclude whether the variability in decoder output is due to measurement noise, spontaneous neural activity, or variability in motor behavior (such as changes in force or coordination of pressing). Assessing the sources of variability in decoder output is a key component of modeling decoded neurofeedback that future work must address.

3.4.1 Conclusions

In this work we show that decoded neurofeedback performance is significantly correlated to decoder accuracy, and we systematically determine the parameter settings needed to optimize that decoder accuracy. We modeled neurofeedback performance using simulations based on real brain data, compared this with human performance with the same brain data, and finally compared it with real neurofeedback performance. We observed similar performance in all cases, validating the accuracy of the simulations. We found a quantitative representation of the high level of dependence of neurofeedback performance on success threshold and decoder accuracy. These results will help improve the robustness of decoded neurofeedback experiments, both by identifying proper preprocessing parameters and by identifying likely 'non-responder' participants prior to training. The simulation paradigm validated here can be used in future research to pre-emptively and efficiently sweep the parameter space to optimize the design of decoded neurofeedback experiments.

Chapter 4

Neural and behavioral evidence for differential plasticity of individual fingers[1]

Abstract

Previous work has shown that fMRI activity patterns associated with individual fingers can be shifted by temporary impairment of the hand (e.g. by gluing two of the fingers together for 24 hours). Here, we investigated whether these neural activity patterns could be modulated endogenously and whether any behavioral changes result from modulation of these patterns. We used decoded neurofeedback in healthy individuals to encourage participants to shift the neural activity pattern of the middle finger towards the index finger, and the ring finger towards the little finger. We first mapped out the neural activity patterns for digits 2-5 of the right hand in an fMRI 'finger localizer' session. Then, in 3 subsequent decoded neurofeedback sessions, participants were rewarded during presses of the middle and ring fingers according to a real-time pattern overlap metric for each finger. A force-sensitive keyboard was used to ensure

[1] This chapter, in full, is a manuscript entitled "Neural and behavioral evidence for differential plasticity of individual fingers" to be submitted for publication. Oblak, Ethan F.; Lewis-Peacock, Jarrod A.; Sulzer, James S. The dissertation author was the primary author of the manuscript. The author was responsible for conceptualization and design of the experiment, development of tools for the experiment (force-sensitive MRI compatible keyboard and real-time fMRI analysis software), fMRI data collection, analysis, and visualization of this research.

that participants were not consciously altering their finger coordination patterns. We found evidence that participants could learn to shift the activity pattern of the 4th digit (ring finger) but not of the 3rd digit (middle finger). Increased variability of these fMRI patterns during the finger localizer session was associated with the ability of participants to modulate them during decoded neurofeedback. Participants also showed an increased preference for the ring finger but not for the middle finger in a post-neurofeedback motor task. Our results show that neural activity and behaviors associated with the ring finger are more readily modulated than those associated with the middle finger. These results have broader implications for rehabilitation of individual finger movements, which may be limited or enhanced by individual finger plasticity after neurological injury.

4.1 Introduction

Movements of individual fingers have distinct neural activity patterns that can be measured using multi-voxel pattern analysis (MVPA) of fMRI data from sensorimotor cortex [18, 19]. These MVPA finger representations can be shifted by gluing two of the fingers together for a short period of time, and this temporary impairment correlates with behavioral deficits recorded after un-gluing the fingers [42]. In this study, we investigated whether these neural representations could be causally shifted without using a physical intervention such as gluing. Instead of physically attaching two fingers together, we used a technique known as associative decoded neurofeedback [3]. This technique was used by Amano et al. (2016) [3] to associate a neutral visual stimulus (grey orientation grating)

with another visual stimulus (colored orientation grating). In this study, we used associative decoded neurofeedback to associate presses of one finger (either the middle or ring finger) with the outwardly adjacent finger (index or little finger). This manipulation was intended to match the neural changes found by Kolasinski et al. (2016) [42], in which the representations of the middle and ring finger were shifted apart, and the representations of the ring and little finger moved closer together.

The complete experiment consisted of 4 fMRI sessions: a fMRI pattern localizer session followed by 3 decoded neurofeedback sessions (Fig 4.1A). During the pattern localizer, participants pressed each of the fingers an equal number of times, whereas during decoded neurofeedback participants pressed either the middle or ring finger. Pressing behavior was controlled using a force-sensitive keyboard to ensure participants exerted the same amount of force during each trial (Fig 4.1B). Motor behavior was assessed before and after each fMRI session using a rapid reaction time task (Fig 4.1C). This task captured behavioral changes resulting from any short-term plasticity associated with the neurofeedback manipulation as well as any changes due to repeated presses of only the middle and ring fingers over the course of each neurofeedback session. Somatosensory ability was assessed before and after the full experiment using a tactile temporal order judgment task in which adjacent finger pairs were stimulated in quick succession (Fig 4.1D). This assessment determined if any changes in tactile discrimination ability occurred due to neurofeedback.

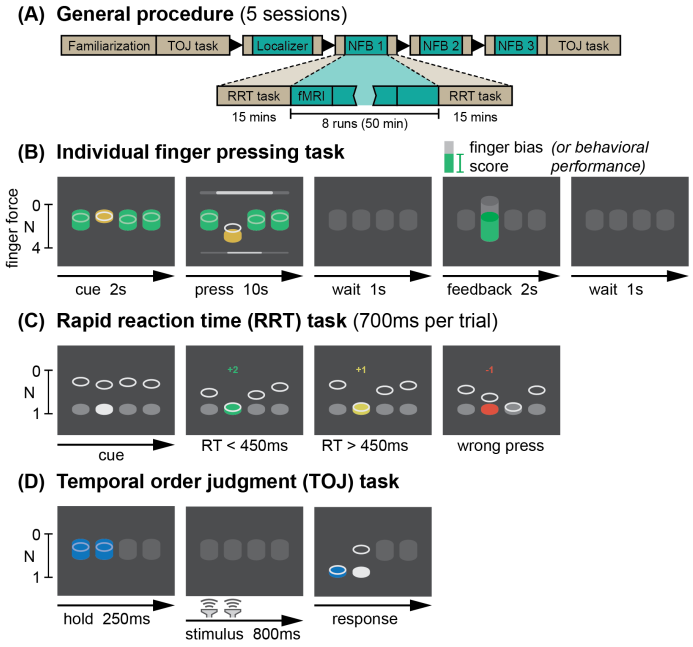

Figure 4.1: **Experimental design. (A)** The 5-session experiment consisted of behavioral familiarization, a finger localizer fMRI session, and 3 neurofeedback sessions. Each fMRI session included behavioral pre- and post-tests. **(B)** An individual finger pressing task was used as the basis for the localizer and neurofeedback sessions. Participants were required to make individual presses with one of 4 fingers (index, middle, ring, or little) while maintaining constant pressure on all other keys. At the end of each trial, feedback was presented related to their motor behavior (localizer session) or their ability to bias the fMRI patterns related to finger presses (neurofeedback sessions). **(C)** A rapid reaction time (RRT) task was used to assess motor confusion before and after each fMRI session. Participants were encouraged to make rapid presses (reaction time below 450ms) through a point system. **(D)** A temporal order judgment (TOJ) task was used to assess the hand representation of participants before and after the entire neurofeedback protocol. During a 800ms stimulus blank period, a brief vibrotactile stimulus was delivered to 2 adjacent fingers in rapid succession. Participants then judged which of the two stimuli happened first.

4.2 Results

4.2.1 Differential modulation of neural patterns related to individual fingers

Presses of each of the ring and middle fingers were associated with a 'bias score' intended to shift their representations based on real-time decoded patterns of fMRI activity (Fig 4.2A). After each 10-sec trial of pressing, this score was displayed to participants as a feedback thermometer (Fig 4.1B). For the middle finger, the score was higher when the real-time decoded pattern appeared more similar to the index finger, and lower when the decoded pattern was more similar to the ring finger. For the ring finger, the score increased with little finger evidence and decreased with middle finger evidence. Participants received monetary reward related to their ability to increase the bias scores for each finger, up to a total of $30 per session.

Participants were unable to reliably increase the middle finger bias score above the baseline level from the pattern localizer during any of the neurofeedback sessions (Dunnett's post-hoc test by session: 1, p=0.940; 2, p=0.860; 3, p=0.975) (Fig 4.2B). However, participants were able to increase the ring finger bias score above baseline: bias scores for the ring finger were significantly above chance for sessions 1 (p=0.013) and 3 (p=0.049), and trending towards significance for session 2 (p=0.082) (Fig 4.2C).

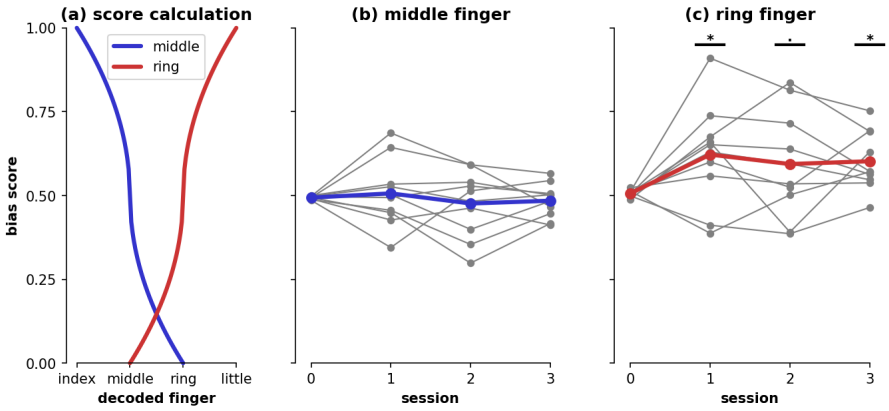

Figure 4.2: **Individual finger pattern bias modulation. (A)** Feedback bias score calculation for middle (blue) and ring (red) fingers. Sample middle finger scores given for decoded fingers from index (maximum score) to ring (minimum score). Sample ring finger scores given from middle (minimum) to little (maximum). See Methods for bias score calculation details. **(B)** Mean middle finger bias scores by session (0: pattern localizer; 1-3: neurofeedback sessions). Grey dots indicate means for each participant, blue dots indicate means across the entire group. **(C)** Mean ring finger bias scores by session. Statistical differences relative to the pattern localizer session are indicated at $p<0.1$ (.) and $p<0.05$ (*).

4.2.2 Baseline variability predicts neuromodulation ability

When bias scores were taken from the pattern localizer session for all participants, mean bias scores were similar for the middle (0.494) and ring (0.507) fingers, but variability (standard deviation) was on average larger for the ring (SD=0.038) than the middle (SD=0.027) (Fig 4.3A). This variability was not reliably different for each finger when compared within subject ($t_{(9)}$=1.67, p=0.13), but did correlate with individual participants' abilities to increase each finger's bias score (Spearman's rho=0.39, p=0.036) (Fig. 4.3B).

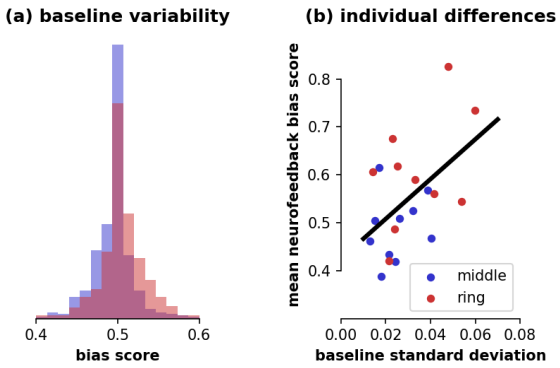

Figure 4.3: **Baseline variability of individual finger patterns. (A)** Distributions of bias scores for middle (blue) and ring (red) fingers for all participants during the baseline pattern localizer session. **(B)** Relationship between individual participant bias pattern variability during the pattern localizer session (standard deviation) and mean bias score achieved during neurofeedback sessions for each finger.

4.2.3 Differential modulation of finger preference

Motor behavior was assessed before and after each fMRI session in a rapid reaction time task. The pressing order in this task was randomized to have an equal number of presses of each finger and an equal number of transitions between each possible two-finger combination. We considered two factors that would influence participants' pressing behavior: the neurofeedback manipulation as well as the fact that participants would only be pressing the middle and ring fingers throughout each fMRI neurofeedback session.

To assess the effect of motor repetition, we measured finger preference as the proportion of total presses by each finger during each testing session (Fig 4.4A). We hypothesized that participants would have increased preference

for the middle and ring fingers after each neurofeedback session due to motor repetition. After the first neurofeedback session, preference for the ring finger significantly increased ($t_{(9)}$=3.82, p=0.004) and preference for the little finger significantly decreased ($t_{(9)}$=-3.50, p=0.007). Preference for the index finger was trending towards a decrease ($t_{(9)}$=-1.87, p=0.094), and preference for the middle finger did not significantly increase ($t_{(9)}$=1.56, p=0.15). After the second neurofeedback session, preference for the little finger was trending towards a decrease ($t_{(9)}$=-2.19, p=0.056) but no other near-significant results were found (all other p>0.1). After the third neurofeedback session, preferences were unchanged (all p>0.1).

To assess the neurofeedback manipulation, we measured motor confusion between finger pairs using the number of mis-presses within each finger pair. A mis-press was defined as a press that was supposed to be with one finger of the pair, but was instead performed with the other finger of the pair. We hypothesized that the neurofeedback manipulation would result in increased confusion (mis-presses) within index-middle and ring-little finger combinations, and decreased confusion within the middle-ring finger pair, as was found by Kolasinski et al. (2016) [42]. However, there were no significant differences between the change in mis-presses in any finger pairs (Tukey's HSD, all sessions, all finger pair contrasts p>0.1) (Fig 4.4B). We also assessed somatosensory ability before and after the entire experiment using the just noticeable difference (JND) in tactile discrimination within each finger pair. There were no significant differences between the performance changes in any finger pairs (Tukey's HSD,

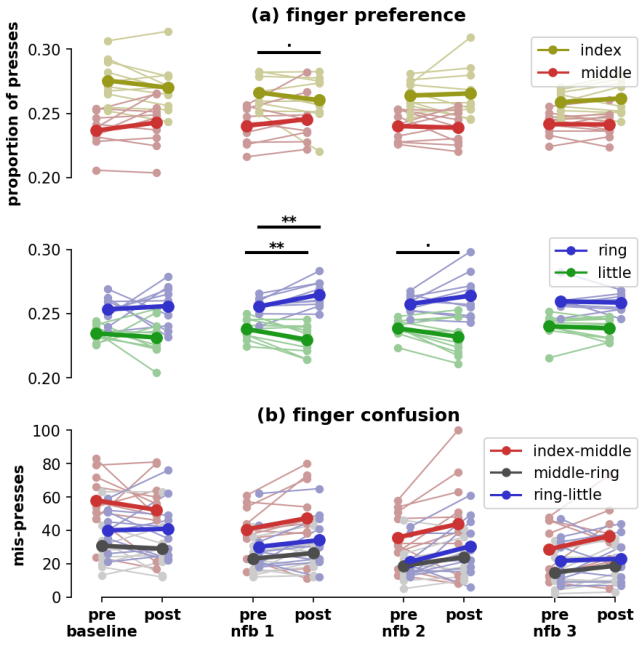

Figure 4.4: **Finger pressing behavior before and after each fMRI scan. (A)** Finger preference in pre and post-fMRI rapid reaction time tests, as a proportion of the total number of presses. Faded colors indicate each participant's performance, solid colors indicate means across the group. Within-finger statistical differences from pre to post-test are shown at $p<0.1$ (.) and $p<0.01$ (**). **(B)** Confusion between fingers in pre and post-fMRI rapid reaction time tests. Mis-presses are assigned to a finger pair when the target finger was one of the fingers of the pair, but the other finger in the pair was pressed instead.

all finger pair contrasts $p>0.1$).

4.3 Discussion

In this study both neural activity and behavior associated with the ring finger were manipulated, while the same was not possible for the middle finger.

Participants implicitly learned to shift the neural representation of the ring finger toward that of the little finger, but on average were unable to shift the representation of the middle finger toward the index finger. The baseline variability of participants' individual finger representations were nevertheless predictive of their ability to bias each finger's representation. After the first neurofeedback session, participants also showed increased preference for the ring finger and decreased preference for the little finger, although no such preference shifts occurred with the middle or index fingers. These results imply greater plasticity for the ring finger than the middle finger, which is supported by the natural variability of these fingers' representations.

Our results showing differential plasticity are complementary to those found by Kolasinski et al. (2016) [42]: although they glued the index and middle fingers together and hypothesized plasticity changes within those fingers, they only found evidence of shifts in the representation of the ring finger, with the strongest behavioral changes also found within the ring and little fingers. These results also agree with animal experiments in which electrophysiologically-recorded signals were easier to control when they aligned with more naturally varying neural activity patterns, rather than along an unnatural manifold [59]. In decoded neurofeedback, there is also within-subject evidence that certain patterns are easier to regulate than others. In a crossover design, Cortese et al. (2017) [13] found that while participants could learn to both up and down-regulate patterns related to confidence judgments, upregulation of these patterns was easier and had a stronger effect on subsequent learning of downregulation compared to the

reversed condition. The relationship discovered between neural pattern variability and learning ability supports our previous findings in which pattern localizer data was able to predict participants' ability in a subsequent decoded neurofeedback task [54]. By examining baseline variability of patterns, future studies may be able to determine the feasibility of controlling specific neural patterns.

This work also represents the first decoded neurofeedback study to target motor behaviors [76]. Furthermore, it is the first fMRI neurofeedback study to target individual fingers, rather than modulating overall sensorimotor cortex activity [8, 6]. These results also have implications for rehabilitation of individual finger movements after stroke. The strength and coordination of individual finger movements are impaired after stroke, recovering significantly through the first year post-stroke but often leaving chronic deficits [85]. Recent work has suggested that this recovery and subsequent chronic impairment can be tracked through MVPA of individual finger representations [84], although the to-date published results of the fMRI data from this study report only average region-of-interest analyses [20]. Although advanced robotic techniques exist for improving finger individuation [71, 69], our approach does not require external physical stimulus, and thus represents an endogenous method for altering finger individuation. Unlike conventional therapy which requires participants to be aware of their movements, the implicit approach of decoded neurofeedback may make therapy easier to administer. This approach has a long history of use in altering spinal reflexes in rats [10], non-human primates [83], and humans [72]. More recently, it been used with success to improve gait in spinal cord injury pa-

tients without requiring conscious effort [73], showing promise for rehabilitation. As our technique shows the ability for participants to gain control over the neural activity patterns related to individual fingers, we suggest that we may be able to improve individual finger coordination after stroke through the use of decoded neurofeedback. The present work implies that greater plasticity leads to greater learning to shift each pattern. There exists an acute post-stroke period in which increased plasticity leads to better recovery [90, 89]. By timing the decoded neurofeedback training in accordance with this increased plasticity, we may be able to significantly boost recovery post-stroke.

A major limitation of the study is that there was no observable change in the targeted finger behavior that could be conclusively linked to the neurofeedback manipulation. This is not unlike operant conditioning of spinal reflexes: Thompson et al. (2009) [72] did not find any changes in gait due to conditioning in healthy individuals, and it was only later after studying patients in which significant gait improvements were found [73]. Therefore, it may be necessary to perform decoded neurofeedback training on patients with significant deficits to observe any changes in finger behavior. Furthermore, a major behavioral confound in our study (pressing of only 2 of the fingers during neurofeedback training) may have masked any small effects of decoded neurofeedback. An ideal experiment would involve training of all 4 fingers; however, this would involve learning twice as many patterns as the present experiment. As this is the first study of its kind, we compromised between too little variation (e.g. only training 1 finger) and presenting participants with too dofficult of a task (training all 4

fingers). This allowed us to have a within-subject control (training of 2 different fingers) without presenting a potentially impossible task to participants. Future work should include all possible fingers, with careful consideration during the training schedule to ensure participants can learn to control the multitude of patterns. We also found no changes in sensory behavior, which may be due to the neurofeedback task being primarily a motor task. Future studies could include vibrotactile stimulation during the neurofeedback phase to enhance changes in sensory behavior.

Overall, the first attempt at decoded neurofeedback in sensorimotor cortex demonstrated both promise and limitations for the technique. Our results show that certain patterns and behaviors may be difficult to manipulate in certain fingers or in individuals with decreased sensorimotor cortex plasticity. However, our results were able to support existing literature and provide a unique window into the plasticity and representations of individual finger movements in humans. Furthermore, we present a unique technique that may be able to enhance rehabilitation of individual fingers without requiring physical intervention at the limb or conscious effort from patients.

4.4 Methods

4.4.1 Participants

14 healthy participants were recruited for the experiment in accordance with the University of Texas Institutional Review Board. Informed consent was obtained from all participants. 1 participant became uncomfortable during the

first fMRI session and did not continue in the experiment. 2 participants completed the first fMRI session but elected not to continue in the experiment. 1 additional participant completed the familiarization session outside of the MRI scanner but did not continue the experiment due to illness. Thus, 10 participants completed the experiment and remained in the final analysis (4 female, average age 25.5 years, SD=5.2).

4.4.2 Apparatus

Finger presses were recorded from the index, middle, ring, and little fingers of the right hand using a custom force-sensitive keyboard at 120Hz. For tests outside of the MRI scanner, the keyboard (force sensor: TE FS20) was placed on a desk, and visual instructions and feedback were presented on a laptop screen using Python and Pygame. For tests inside the MRI scanner, the keyboard (force sensor: Honeywell FSS015) was affixed to a wooden board, which lay on the participant's lap, and visual instructions and feedback were provided through a back-projection screen. For vibrotactile stimulus, two vibrotactile stimulators (Soberton E-12041808) were placed on top of the force-sensitive keyboard.

4.4.3 Imaging parameters

Participants were scanned in a Siemens Skyra 3T scanner with a 32-channel head coil. For all fMRI sessions, the same EPI sequence was used (TR=2s; 36 slices; in-plane resolution 2.3x2.3mm; 100x100 matrix size; 2.15mm

slice thickness; 0.15mm slice gap; 2x multiband factor). After auto-alignment to the AC-PC plane, a manual adjustment was performed to ensure coverage of the motor cortex. The same manual adjustment parameters were applied to the subsequent neurofeedback sessions. A high-resolution anatomical scan (MEMPRAGE, 1mm isotropic voxels) was also acquired during the first localizer session to identify the primary sensorimotor cortex (M1+S1) using Freesurfer. Subsequent real-time fMRI scans were rigidly aligned to this template using AFNI's 3dvolreg.

4.4.4 General procedure

The experiment consisted of 5 sessions: 1 familiarization session outside of the MRI scanner, 1 finger pattern localizer session inside the MRI scanner, and 3 decoded neurofeedback sessions inside the MRI scanner. Each fMRI session had a behavioral pre- and post-test. A custom-made force-sensitive keyboard was used inside the MRI scanner to control finger coordination patterns during neurofeedback. We used a within-subject control by providing 2 different types of neurofeedback on alternating trials: one based on index-middle finger coordination and one based on ring-little finger coordination.

4.4.5 Individual finger pressing task

An individual finger pressing task was performed during all fMRI scanning sessions. This task was also performed for 15 minutes during the familiarization session. Each trial of the task consisted of 10 seconds of individual

finger pressing followed by 2 seconds of feedback. Each trial was preceded by a 2 second cue for the target finger, and feedback was both preceded and followed by 1 second wait periods, leading to a 16 second trial duration. In the familiarization and localizer sessions, feedback was related to maintaining normal finger coordination patterns on the individual finger pressing task, while in the neurofeedback sessions, feedback was related to neural activity in sensorimotor cortex. Each fMRI session consisted of 8 runs of 20 trials each, lasting about an hour.

Participants were instructed to press the target finger (one of index, middle, ring, or little) while keeping a constant pressure on the 3 other (non-target) fingers. During the cue and pressing period, the real-time force of each finger was displayed as a grey disk. For the target finger, a yellow target cylinder was visible indicating the target force range. Two types of targets were displayed in alternating order: low force (0.2 to 1.2N) and high force (2.0 to 3.0N). Participants were required to keep the grey finger disk in the target cylinder for 200ms before moving on to the next target. Participants had 10 seconds to hit as many targets as possible, indicated by a timer bar at the bottom of the screen. For each non-target finger, a cylinder was visible indicating a constant force range to maintain (0.2-1.5N). While fingers exerted a force in this range, the non-target cylinder turned green, and the grey disk was hidden by the cylinder; if fingers exerted more or less force than this force range, the cylinder turned red and the real-time force of the finger was visible as a grey disk, either above or below the cylinder depending on whether the force was less or greater than the desired

force range.

Points were tallied during this task based on hitting targets with the target finger and maintaining constant force on the non-target fingers. Specifically, targets were assessed as 'hits' (+1 point, green score message: '+1'), 'misses' (0 points, red score message: 'miss!'), or 'non-target fingers off' (0 points, red score message: 'off!'). Hits were tallied if the target finger remained inside the yellow target cylinder for 200ms and all non-targets fingers remained inside the constant force cylinders. If the target finger entered and exited the target cylinder in less than 200ms, a miss was recorded. If the target was hit but any of the non-target fingers exited their constant force cylinder, then a non-target finger off was recorded. Participants were encouraged to gain at least 15 points each trial. At the beginning of each trial, a grey score bar appeared at top of the screen, at the same width as the timer bar. As targets were hit, the score bar decreased in size, up to a score of 15. After 15 targets were hit, the score bar turned green and increased in size. After 10 seconds of pressing, a feedback thermometer appeared in the position of the target finger, related to the participant's performance during that trial. If at least 15 targets were hit, the feedback thermometer cylinder turned green; if less than 15 targets were hit, the feedback thermometer was grey. Feedback was either related to the number of targets hit (familiarization and finger localizer sessions) or the participant's neural activity during pressing (neurofeedback sessions).

4.4.5.1 Behavioral feedback

In the familiarization and finger localizer sessions, the feedback thermometer was directly related to the number of targets hit. Initially, the maximum height of the thermometer was equivalent to 15 points. For each finger, the maximum score achieved by the participant in that session was used to recalibrate the maximum height of the thermometer. The numerical score was also shown below the feedback thermometer during the feedback period (in green for scores 15 or above or in grey for scores below 15). At the end of each run, the total score over all trials was shown at the bottom of the screen.

4.4.5.2 Individual finger decoding

The fMRI data from the finger localizer task was used to create a finger decoder to be used in the subsequent neurofeedback sessions. Standard preprocessing (rigid body motion correction, detrending, and z-scoring) was performed. The preprocessed fMRI data from the last 6 seconds of pressing was averaged over time for each trial to yield 160 time-averaged trials, 40 per finger. The hand area of the primary sensorimotor cortex was identified in each participant by first training a sparse multinomial logistic regression decoder (SMLR; PyMVPA) on the larger primary sensorimotor cortex (Brodmann areas 4A, 4P, 3A, and 3B identified using Freesurfer), and then selecting only those voxels within a 15mm radius of the center of the hand area. A final SMLR decoder was trained on only these voxels, and exported for use in neurofeedback. For real-time fMRI neurofeedback sessions, each run began with 20 seconds of baseline

rest. At each TR, data was linearly detrended using the current time history and z-scored using the variance estimated from the initial baseline period.

4.4.5.3 Neurofeedback

In neurofeedback sessions, participants were rewarded up to $30 per session for shifting the neural activity pattern of the middle finger towards that of the index, and for shifting the neural pattern of the ring finger towards the little finger. Specifically, the neurofeedback score is summarized in Equation 4.1, where $finger_{reward}$ is the decoder output for the finger adjacent to the target finger that is being rewarded (middle: index; ring: little) and $finger_{punish}$ is the decoder output for the finger adjacent to the target finger that is being punished (middle: ring; ring: middle). Time points used for decoding were identical to the finger localizer task (i.e. the time-averaged fMRI data from the last 6 seconds of pressing).

$$\begin{aligned} score_{raw} &= finger_{reward} - finger_{punish} \\ score_{adjusted} &= 0.5 + 0.5 * sgn(score_{raw}) * |score_{raw}|^{1/2} \end{aligned} \tag{4.1}$$

Participants were simply instructed to regulate their brain activity during pressing to maximize the height of the feedback thermometer ($score_{adjusted}$), and that the neural activity signature would be different for each finger. If they achieved at least 15 points on the individual pressing task, they saw their neural activity feedback score as a green thermometer, indicating reward proportional to the height of the thermometer; if they did not achieve this minimum score, they

saw their neural activity as a grey feedback thermometer and did not receive reward. Trials were blocked in groups of 5 repetitions of the same finger (i.e. 5 trials of middle finger presses followed by 5 trials of ring finger presses). The amount of money earned was displayed at the bottom of the screen at the end of each run.

4.4.5.4 Post-hoc calculation of bias scores

To ensure that real-time processing did not skew the bias scores, they were recalculated offline. Variance for z-scoring was estimated using the baseline period at the beginning of each run, as in the neurofeedback sessions. Offline detrending was performed using GLM correction that accounted for the explicit finger presses during the neurofeedback sessions [43]. The same SMLR decoder and feedback calculation equation as in the neurofeedback sessions were then applied.

4.4.6 Behavioral assessment: rapid reaction time task

We assessed short-term plasticity associated with each neurofeedback session using a motor confusion task in which participants performed rapid button presses (700ms between presses) of pseudorandomly cued fingers. Participants viewed the real-time force of each finger as a grey disk that moved up and down with each finger. Under each finger's disk was a corresponding target grey disk. Every 700ms, one of the target disks would light up white, indicating the finger to press. A selected finger was detected as the first finger to

exceed a force of 1N. Participants were encouraged to make rapid presses of the correct finger through a point system. If the incorrect finger was selected, the target disk lit up red and a score of -1 point was tallied. If the correct finger was pressed with a reaction time greater than 450ms, the target disk lit up yellow and a score of +1 point was tallied. If the correct finger was pressed with a reaction time faster than 450ms, the target disk lit up green and a score of +2 points was tallied. At the end of each run (217 presses), the participant's score was displayed. The press order in each run was randomized to ensure an equal number of each possible finger transition (18 transitions for each of the 12 possible finger transitions). Participants performed 6 runs of this task (approximately 15 minutes) immediately before and after each fMRI session in a room adjacent to the scanner.

4.4.7 Behavioral assessment: temporal order judgment task

Long-term changes in hand representation were assessed using a temporal order judgment task in which participants had to judge which of two adjacent fingers received a vibrotactile stimulus first. This task was conducted during the familiarization session, as well as after the final neurofeedback session. Each run of the task targeted 2 adjacent fingers (index-middle, middle-ring, or ring-little). Participants rested their fingers on top of vibrotactile stimulators (Soberton E-12041808) which lay on the force-sensitive keyboard. The real-time applied force of the 2 targets fingers were displayed as grey disks. To begin each trial, participants were required to apply a constant force on the

stimulators (between 0.2N and 0.5N, indicated by a blue cylinder) for 250ms. After this, the display went blank for 800ms. During this blank period, the two fingers were stimulated one after the other (20 ms duration, 200 Hz sinusoidal pulse), with possible inter-stimulus intervals (ISIs) of +400, –400, +250, –250, +180, –180, +120, –120, +70, –70, +30 or 30ms where, by convention, a positive ISI indicates the rightward digit was stimulated first. The onset of the first pulse was randomly jittered, starting between 150ms and 350ms after the beginning of the blank period. After the blank period, a target disk appeared in white for each finger, and the real-time force of each finger also re-appeared as a grey disk. Participants were instructed to select the finger which was first stimulated. Selections were detected as the first finger to exceed a force of 1N. The selected target lit up blue, and a blue asterisk appeared above the selected finger; however, no feedback was given as to whether the selection was correct. At this point, the two blue cylinders appeared again, and the next trial began once the participant kept the constant (between 0.2N and 0.5N) force on the stimulators for 250ms. At the end of each run (120 trials, 10 per ISI), summary accuracy over the run was displayed to participants. In each session of the temporal order judgment task, participants completed 9 runs total (3 for each finger pair) in pseudorandomized order, lasting about 45 minutes. Participants listened to pink noise over headphones to mask any auditory cues from the vibrotactile stimulators.

4.4.8 Statistical analyses

Participants' ability to bias patterns was assessed for each of the middle and ring fingers using a linear mixed effects model (nlme in R [56]) with participant as a random effect. Bias scores were recalculated offline, taking into account the explicit finger pressing task during neurofeedback, to ensure that they were not skewed. Dunnett's post-hoc test ($\alpha <$0.05) was performed to compare bias scores during each of the neurofeedback sessions to the baseline level measured during the pattern localizer session. The relationship between baseline variability and participants' ability to bias patterns was calculated using Spearman's rho. Significance was established using 10,000 bootstrap correlations selecting either the ring or middle finger randomly for each participant, with the p-value calculated as the proportion of iterations with rho$<$0.

Paired t-tests were used to assess changes in finger preference at each neurofeedback session Significance was assessed using Bonferroni adjusted alpha levels of 0.0125 per finger (0.05/4). Changes in motor confusion between finger pairs at each neurofeedback session was assessed by creating a linear mixed effects model for each session with participant as a random effect. Tukey's post-hoc test ($\alpha <$0.05) was used to determine if there were differences between finger pairs. A similar linear mixed effects model was created for assessing changes in tactile discrimination behavior due to all 3 neurofeedback sessions.

Chapter 5

Conclusions and future work

5.1 Conclusions

This work not only provides a systematic investigation into optimizing fMRI neurofeedback parameters, but also lays the foundation for rehabilitation of individual finger movements. The major findings of this work are found below:

1. simulated fMRI neurofeedback reveals optimal feedback parameters for learning with both conscious and unconscious strategies

    i. continuous feedback of the delayed and blurred fMRI signal is superior when conscious strategies are used

    ii. when there are too many possible conscious strategies to try, or when a conscious strategy is not known, then intermittent feedback is superior as we must rely on unconscious strategies

2. individual finger movements can be decoding in real-time from fMRI

    i. individual finger movements (index-ring-middle-little) can be decoded with 85% accuracy from 6-sec of fMRI data, using a decoder constructed using one session (approximately 1 hour) of fMRI data

ii. with 3T BOLD fMRI, a sparse logistic regression decoder can select the relevant finger-related brain regions from the larger sensorimotor cortex (primary motor cortex and primary somatosensory cortex), but attempting to restrict decoding to either motor or somatosensory areas can significantly impact decoding accuracy (up to 30%)

iii. data from the decoder construction session can be used to predict participants' performance in a subsequent neurofeedback session

3. real-time fMRI patterns are more easily shifted in the ring finger than the middle finger

   i. participants learned to shift the fMRI pattern of the ring finger towards the little finger, but were unable to shift the pattern of the middle finger towards the index finger

   ii. participants' motor behavior was influenced in the ring-little finger pair but not in the index-middle or middle-ring finger pairs

   iii. natural variability in the fMRI patterns for each finger helped explain participants' ability to regulate them

   iv. decoded neurofeedback of individual finger patterns was shown to be possible, opening an avenue for neurally guided physical therapy of individual finger movements

5.2 Future work

Future work will apply these principles to stroke rehabilitation, first by mapping the neural correlates of force coordination patterns within the MRI scanner and subsequently applying the same decoded neurofeedback strategy from healthy participants to stroke patients. Because MVPA maps of individual fingers may be weak in stroke patients, future work will attempt to align the strong finger maps of healthy participants, recorded during our current studies, to the weakened patterns of stroke patients. This procedure, called hyperalignment [32], has already begun to be used in decoded neurofeedback studies [70], and may provide a pathway to restore healthy coordination in stroke patients.

Further studies in healthy individuals will expand from individual finger movements to the study of sequences of finger movements. Because the MVPA maps of sequential movements increase in strength with practice [79], we believe that sequences of finger presses could be learned, or strengthened, using decoded neurofeedback of the neural representation of those sequences. This, combined with hyperalignment of skills between individuals, would provide an avenue to transfer the abilities learned by one person into the brain of another.

This work represents the early stages of neurally guided physical therapy. The fundamental limitations of fMRI signal quality make effective clinical interventions difficult to imagine at this time. The technique of fMRI neurofeedback is likely relegated to scientific investigation for now, teaching us about the neural mechanisms of recovery but falling short of offering a clinical solution. Notwithstanding the cost and comfort disadvantages of the MRI scanner, our

ability to record and decode individual finger movements is still limited. Future work should aim for 100% accurate decoding of finger movements, which may require a combinination of advanced signal processing, higher strength magnetic fields, or new fMRI pulse sequences. More effective neural recording techniques, beyond traditional fMRI, may be necessary to achieve such accurate decoding of sensorimotor cortex activity. Although intracranial electrodes currently offer increasingly detailed signals, their invasiveness makes them an impractical solution. Safe implantation of such electrodes will, for the time being, be limited to small patient populations. Within the MRI scanner, however, there is still potential for improved neural recording techniques - for example, by directly recording the magnetic activity of neurons [4]. Investigation into these techniques is still ongoing, but these MRI sequences may eventually become more effective than current fMRI methods.

As neural recording techniques continue to improve, the fundamentals of this work will be ever-important. The temporal characteristics of newly-discovered signals should be carefully considered before including them in a neurofeedback loop, either continuously or intermittently. Even if we are able to record extremely detailed neural activity, we must also consider constraints on neuroplasticity: if natural variability does not exist in a certain signal, it may be difficult or impossible to modulate. Increasing the reliability of our recordings (e.g. by increasing the accuracy of neural decoding from sensorimotor cortex) will help us better determine these limitations: by minimizing measurement noise, we can more confidently conclude which failures in neurofeedback are due to the

limitations of neuroplasticity and not simply poor signal quality.

In order to rewire the brain to its maximum potential after neurological injury, it is clear that neural activity and neuroplastic limitations should be considered. However, our limited view into the brain with current neuroimaging techniques may be insufficient to improve rehabilitation beyond traditional therapy. Future work in patients will compare fMRI neurofeedback to biofeedback calculated solely from a force-sensitive keyboard. It is possible that training finger coordination using recordings from a force-sensitive keyboard could lead to clinical improvements without requiring the use of the MRI scanner. However, pre- and post-training fMRI scans should still be performed to examine the effect of force biofeedback training on the neural patterns of individual fingers. Despite neuroimaging limitations, we may still find that fMRI neurofeedback has an advantage over force biofeedback by avoiding maladaptive neuroplasticity; any potential advantages of neurofeedback over traditional physical therapy will only continue to grow alongside the development of novel neuroimaging and signal processing techniques.

Bibliography

[1] Arjen Alink, Alexandra Krugliak, Alexander Walther, and Nikolaus Kriegeskorte. fMRI orientation decoding in V1 does not require global maps or globally coherent orientation stimuli. *Frontiers in Psychology*, 4, 2013.

[2] Brendan Z Allison and Christa Neuper. Could anyone use a BCI? In *Brain-computer interfaces*, pages 35–54. Springer, 2010.

[3] Kaoru Amano, Kazuhisa Shibata, Mitsuo Kawato, Yuka Sasaki, and Takeo Watanabe. Learning to associate orientation with color in early visual areas by associative decoded fMRI neurofeedback. *Current Biology*, 26(14):1861–1866, 2016.

[4] PA Bandettini, N Petridou, and J Bodurka. Direct detection of neuronal activity with mri: fantasy, possibility, or reality? *Applied Magnetic Resonance*, 29(1):65–88, 2005.

[5] Benjamin Blankertz, Claudia Sannelli, Sebastian Halder, Eva M Hammer, Andrea Kübler, Klaus-Robert Müller, Gabriel Curio, and Thorsten Dickhaus. Neurophysiological predictor of SMR-based BCI performance. *Neuroimage*, 51(4):1303–1309, 2010.

[6] Maria L Blefari, James Sulzer, Marie-Claude Hepp-Reymond, Spyros Kollias, and Roger Gassert. Improvement in precision grip force control with

self-modulation of primary motor cortex during motor imagery. *Frontiers in behavioral neuroscience*, 9:18, 2015.

[7] Geoffrey M Boynton, Stephen A Engel, Gary H Glover, and David J Heeger. Linear systems analysis of functional magnetic resonance imaging in human V1. *The Journal of Neuroscience*, 16(13):4207–4221, 1996.

[8] Signe Bray, Shinsuke Shimojo, and John P O'Doherty. Direct instrumental conditioning of neural activity using functional magnetic resonance imaging-derived reward feedback. *Journal of Neuroscience*, 27(28):7498–7507, 2007.

[9] Andre Russowsky Brunoni, Michael A Nitsche, Nadia Bolognini, Marom Bikson, Tim Wagner, Lotfi Merabet, Dylan J Edwards, Antoni Valero-Cabre, Alexander Rotenberg, Alvaro Pascual-Leone, et al. Clinical research with transcranial direct current stimulation (tDCS): challenges and future directions. *Brain stimulation*, 5(3):175–195, 2012.

[10] XIANG YANG Chen and JONATHAN R Wolpaw. Operant conditioning of h-reflex in freely moving rats. *Journal of Neurophysiology*, 73(1):411–415, 1995.

[11] Mark Chiew, Stephen M LaConte, and Simon J Graham. Investigation of fMRI neurofeedback of differential primary motor cortex activity using kinesthetic motor imagery. *Neuroimage*, 61(1):21–31, 2012.

[12] Aurelio Cortese, Kaoru Amano, Ai Koizumi, Mitsuo Kawato, and Hakwan Lau. Multivoxel neurofeedback selectively modulates confidence without changing perceptual performance. *Nature communications*, 7:13669, 2016.

[13] Aurelio Cortese, Kaoru Amano, Ai Koizumi, Hakwan Lau, and Mitsuo Kawato. Decoded fmri neurofeedback can induce bidirectional confidence changes within single participants. *NeuroImage*, 149:323–337, 2017.

[14] Anders Dale, Bruce Fischl, and Martin I. Sereno. Cortical surface-based analysis: I. segmentation and surface reconstruction. *NeuroImage*, 9(2):179 – 194, 1999.

[15] Megan T deBettencourt, Jonathan D Cohen, Ray F Lee, Kenneth A Norman, Nicholas B Turk-Browne, et al. Closed-loop training of attention with real-time brain imaging. *Nature neuroscience*, 18(3):470, 2015.

[16] Megan T deBettencourt, Nicholas B Turk-Browne, and Kenneth A Norman. Neurofeedback helps to reveal a relationship between context reinstatement and memory retrieval. *bioRxiv*, page 355727, 2018.

[17] Christopher R deCharms, Fumiko Maeda, Gary H Glover, David Ludlow, John M Pauly, Deepak Soneji, John DE Gabrieli, and Sean C Mackey. Control over brain activation and pain learned by using real-time functional MRI. *Proceedings of the National Academy of Sciences of the United States of America*, 102(51):18626–18631, 2005.

[18] Jörn Diedrichsen, Tobias Wiestler, and John W Krakauer. Two distinct ipsilateral cortical representations for individuated finger movements. *Cerebral Cortex*, 23(6):1362–1377, 2012.

[19] Naveed Ejaz, Masashi Hamada, and Jörn Diedrichsen. Hand use predicts the structure of representations in sensorimotor cortex. *Nature neuroscience*, 18(7):1034, 2015.

[20] Naveed Ejaz, Jing Xu, Meret Branscheidt, Benjamin Hertler, Heidi Schambra, Mario Widmer, Andreia V Faria, Michelle D Harran, Juan C Cortes, Nathan Kim, et al. Evidence for a subcortical origin of mirror movements after stroke: a longitudinal study. *Brain*, 141(3):837–847, 2018.

[21] Kirsten Emmert, Rotem Kopel, Yury Koush, Raphael Maire, Pascal Senn, Dimitri Van De Ville, and Sven Haller. Continuous vs. intermittent neurofeedback to regulate auditory cortex activity of tinnitus patients using real-time fMRI-a pilot study. *NeuroImage: Clinical*, 14:97–104, 2017.

[22] Nathan Evans, Steven Gale, Aaron Schurger, and Olaf Blanke. Visual feedback dominates the sense of agency for brain-machine actions. *PloS one*, 10(6):e0130019, 2015.

[23] Christopher L Friesen, Timothy Bardouille, Heather F Neyedli, and Shaun G Boe. Combined action observation and motor imagery neurofeedback for modulation of brain activity. *Frontiers in human neuroscience*, 10:692, 2017.

[24] C Randy Gallistel and John Gibbon. Time, rate, and conditioning. *Psychological review*, 107(2):289, 2000.

[25] James S Gao, Alexander G Huth, Mark D Lescroart, and Jack L Gallant. Pycortex: an interactive surface visualizer for fMRI. *Frontiers in neuroinformatics*, 9:23, 2015.

[26] Gary H Glover. Deconvolution of impulse response in event-related bold fMRI. *Neuroimage*, 9(4):416–429, 1999.

[27] Sebastian Halder, Balint Varkuti, Martin Bogdan, Andrea Kübler, Wolfgang Rosenstiel, Ranganatha Sitaram, and Niels Birbaumer. Prediction of brain-computer interface aptitude from individual brain structure. *Frontiers in human neuroscience*, 7, 2013.

[28] Eva Maria Hammer, Sebastian Halder, Benjamin Blankertz, Claudia Sannelli, Thorsten Dickhaus, Sonja Kleih, Klaus-Robert Müller, and Andrea Kübler. Psychological predictors of SMR-BCI performance. *Biological psychology*, 89(1):80–86, 2012.

[29] Michael Hanke, Yaroslav O Halchenko, Per B Sederberg, Stephen José Hanson, James V Haxby, and Stefan Pollmann. PyMVPA: a python toolbox for multivariate pattern analysis of fMRI data. *Neuroinformatics*, 7(1):37–53, 2009.

[30] James V Haxby, Andrew C Connolly, and J Swaroop Guntupalli. Decoding neural representational spaces using multivariate pattern analysis. *Annual*

review of neuroscience, 37:435–456, 2014.

[31] James V Haxby, M Ida Gobbini, Maura L Furey, Alumit Ishai, Jennifer L Schouten, and Pietro Pietrini. Distributed and overlapping representations of faces and objects in ventral temporal cortex. *Science*, 293(5539):2425–2430, 2001.

[32] James V Haxby, J Swaroop Guntupalli, Andrew C Connolly, Yaroslav O Halchenko, Bryan R Conroy, M Ida Gobbini, Michael Hanke, and Peter J Ramadge. A common, high-dimensional model of the representational space in human ventral temporal cortex. *Neuron*, 72(2):404–416, 2011.

[33] John-Dylan Haynes and Geraint Rees. Predicting the orientation of invisible stimuli from activity in human primary visual cortex. *Nature neuroscience*, 8(5):686–691, 2005.

[34] Okihide Hikosaka, Kae Nakamura, Katsuyuki Sakai, and Hiroyuki Nakahara. Central mechanisms of motor skill learning. *Current opinion in neurobiology*, 12(2):217–222, 2002.

[35] Tsung-Ren Huang. Hebbian plasticity for improving perceptual decisions. *arXiv preprint arXiv:1612.03270*, 2016.

[36] David H Hubel and Torsten N Wiesel. Receptive fields and functional architecture of monkey striate cortex. *The Journal of physiology*, 195(1):215–243, 1968.

[37] Kevin A Johnson, Karen Hartwell, Todd LeMatty, Jeffrey Borckardt, Paul S Morgan, Koushik Govindarajan, Kathleen Brady, and Mark S George. Intermittent “real-time” fMRI feedback is superior to continuous presentation for a motor imagery task: a pilot study. *Journal of Neuroimaging*, 22(1):58–66, 2012.

[38] Yukiyasu Kamitani and Frank Tong. Decoding the visual and subjective contents of the human brain. *Nature neuroscience*, 8(5):679–685, 2005.

[39] Tal Kenet, Dmitri Bibitchkov, Misha Tsodyks, Amiram Grinvald, and Amos Arieli. Spontaneously emerging cortical representations of visual attributes. *Nature*, 425(6961):954–956, 2003.

[40] Ai Koizumi, Kaoru Amano, Aurelio Cortese, Kazuhisa Shibata, Wako Yoshida, Ben Seymour, Mitsuo Kawato, and Hakwan Lau. Fear reduction without fear through reinforcement of neural activity that bypasses conscious exposure. *Nature Human Behaviour*, 1(6), 2016.

[41] Ai Koizumi, Kaoru Amano, Aurelio Cortese, Kazuhisa Shibata, Wako Yoshida, Ben Seymour, Mitsuo Kawato, and Hakwan Lau. Fear reduction without fear through reinforcement of neural activity that bypasses conscious exposure. *Nature human behaviour*, 1(1):0006, 2017.

[42] James Kolasinski, Tamar R Makin, John P Logan, Saad Jbabdi, Stuart Clare, Charlotte J Stagg, and Heidi Johansen-Berg. Perceptually relevant remapping of human somatotopy in 24 hours. *Elife*, 5:e17280, 2016.

[43] Rotem Kopel, Ronald Sladky, P Laub, Yury Koush, Fabien Robineau, Chloe Hutton, Nikolaus Weiskopf, Patrik Vuilleumier, Dimitri Van De Ville, and Frank Scharnowski. No time for drifting: Comparing performance and applicability of signal detrending algorithms for real-time fmri. *NeuroImage*, 191:421–429, 2019.

[44] Katja Kornysheva and Jörn Diedrichsen. Human premotor areas parse sequences into their spatial and temporal features. *Elife*, 3:e03043, 2014.

[45] Nikolaus Kriegeskorte and Jörn Diedrichsen. Inferring brain-computational mechanisms with models of activity measurements. *Phil. Trans. R. Soc. B*, 371(1705), 2016.

[46] Balaji Krishnapuram, Lawrence Carin, Mario AT Figueiredo, and Alexander J Hartemink. Sparse multinomial logistic regression: Fast algorithms and generalization bounds. *IEEE transactions on pattern analysis and machine intelligence*, 27(6):957–968, 2005.

[47] Stephen M LaConte, Scott J Peltier, and Xiaoping P Hu. Real-time fmri using brain-state classification. *Human brain mapping*, 28(10):1033–1044, 2007.

[48] Robert Legenstein, Dejan Pecevski, and Wolfgang Maass. A learning theory for reward-modulated spike-timing-dependent plasticity with application to biofeedback. *PLoS computational biology*, 4(10):e1000180, 2008.

[49] Jarrod A Lewis-Peacock and Kenneth A Norman. Multi-voxel pattern analysis of fmri data. *The cognitive neurosciences*, pages 911–920, 2014.

[50] Susan GR McDuff, Hillary C Frankel, and Kenneth A Norman. Multivoxel pattern analysis reveals increased memory targeting and reduced use of retrieved details during single-agenda source monitoring. *Journal of Neuroscience*, 29(2):508–516, 2009.

[51] Hiroyuki Nakahara, Kenji Doya, and Okihide Hikosaka. Parallel cortico-basal ganglia mechanisms for acquisition and execution of visuomotor sequences—a computational approach. *Journal of Cognitive Neuroscience*, 13(5):626–647, 2001.

[52] Kenneth A Norman, Sean M Polyn, Greg J Detre, and James V Haxby. Beyond mind-reading: multi-voxel pattern analysis of fMRI data. *Trends in cognitive sciences*, 10(9):424–430, 2006.

[53] Ethan F Oblak, Jarrod A Lewis-Peacock, and James S Sulzer. Self-regulation strategy, feedback timing and hemodynamic properties modulate learning in a simulated fMRI neurofeedback environment. *PLoS computational biology*, 13(7):e1005681, 2017.

[54] Ethan F Oblak, James S Sulzer, and Jarrod A Lewis-Peacock. A simulation-based approach to improve decoded neurofeedback performance. *NeuroImage*, 195:300–310, 2019.

[55] Jonathan W Peirce. PsychoPy–psychophysics software in Python. *Journal of neuroscience methods*, 162(1-2):8–13, 2007.

[56] Jose Pinheiro, Douglas Bates, Saikat DebRoy, Deepayan Sarkar, and R Core Team. *nlme: Linear and Nonlinear Mixed Effects Models*, 2018. R package version 3.1-137.

[57] Michal Ramot, Shany Grossman, Doron Friedman, and Rafael Malach. Covert neurofeedback without awareness shapes cortical network spontaneous connectivity. *Proceedings of the National Academy of Sciences*, 113(17):E2413–E2420, 2016.

[58] Sergio Ruiz, Korhan Buyukturkoglu, Mohit Rana, Niels Birbaumer, and Ranganatha Sitaram. Real-time fMRI brain computer interfaces: self-regulation of single brain regions to networks. *Biological psychology*, 95:4–20, 2014.

[59] Patrick T Sadtler, Kristin M Quick, Matthew D Golub, Steven M Chase, Stephen I Ryu, Elizabeth C Tyler-Kabara, M Yu Byron, and Aaron P Batista. Neural constraints on learning. *Nature*, 512(7515):423–426, 2014.

[60] Karthik H Shankar and Marc W Howard. A scale-invariant internal representation of time. *Neural Computation*, 24(1):134–193, 2012.

[61] Kazuhisa Shibata, Giuseppe Lisi, Aurelio Cortese, Takeo Watanabe, Yuka Sasaki, and Mitsuo Kawato. Toward a comprehensive understanding of

the neural mechanisms of decoded neurofeedback. *NeuroImage*, 188:539–556, 2019.

[62] Kazuhisa Shibata, Yuka Sasaki, Takeo Watanabe, and Mitsuo Kawato. Response to comment on'perceptual learning incepted by decoded fmri neurofeedback without stimulus presentation'; how can a decoded neurofeedback method (decnef) lead to successful reinforcement and visual perceptual learning? *arXiv preprint arXiv:1612.04234*, 2016.

[63] Kazuhisa Shibata, Takeo Watanabe, Mitsuo Kawato, and Yuka Sasaki. Differential activation patterns in the same brain region led to opposite emotional states. *PLoS biology*, 14(9):e1002546, 2016.

[64] Kazuhisa Shibata, Takeo Watanabe, Yuka Sasaki, and Mitsuo Kawato. Perceptual learning incepted by decoded fMRI neurofeedback without stimulus presentation. *science*, 334(6061):1413–1415, 2011.

[65] Ranganatha Sitaram, Tomas Ros, Luke Stoeckel, Sven Haller, Frank Scharnowski, Jarrod Lewis-Peacock, Nikolaus Weiskopf, Maria Laura Blefari, Mohit Rana, Ethan Oblak, et al. Closed-loop brain training: the science of neurofeedback. *Nature Reviews Neuroscience*, 18(2):86, 2017.

[66] Ranganatha Sitaram, Tomas Ros, Luke Stoeckel, Sven Haller, Frank Scharnowski, Jarrod Lewis-Peacock, Nikolaus Weiskopf, Maria Laura Blefari, Mohit Rana, Ethan Oblak, and James Sulzer. Closed-loop brain training: the science of neurofeedback. *Nature Reviews Neuroscience*, 18(2):86–100, 2017.

[67] James Sulzer, Sven Haller, Frank Scharnowski, Nikolaus Weiskopf, Niels Birbaumer, Maria Laura Blefari, Annette B Bruehl, Leonardo G Cohen, R Gassert, R Goebel, et al. Real-time fMRI neurofeedback: progress and challenges. *Neuroimage*, 76:386–399, 2013.

[68] Richard S Sutton and Andrew G Barto. *Reinforcement learning: An introduction*. Number 1. MIT press Cambridge, 1998.

[69] Hossein Taheri, Justin B Rowe, David Gardner, Vicki Chan, Kyle Gray, Curtis Bower, David J Reinkensmeyer, and Eric T Wolbrecht. Design and preliminary evaluation of the finger rehabilitation robot: controlling challenge and quantifying finger individuation during musical computer game play. *Journal of neuroengineering and rehabilitation*, 11(1):10, 2014.

[70] Vincent Taschereau-Dumouchel, Aurelio Cortese, Toshinori Chiba, JD Knotts, Mitsuo Kawato, and Hakwan Lau. Towards an unconscious neural reinforcement intervention for common fears. *Proceedings of the National Academy of Sciences*, 115(13):3470–3475, 2018.

[71] Kelly O Thielbar, Thomas J Lord, Heidi C Fischer, Emily C Lazzaro, Kristin C Barth, Mary E Stoykov, Kristen M Triandafilou, and Derek G Kamper. Training finger individuation with a mechatronic-virtual reality system leads to improved fine motor control post-stroke. *Journal of neuroengineering and rehabilitation*, 11(1):171, 2014.

[72] Aiko K Thompson, Xiang Yang Chen, and Jonathan R Wolpaw. Acquisition of a simple motor skill: task-dependent adaptation plus long-term change

in the human soleus h-reflex. *Journal of Neuroscience*, 29(18):5784–5792, 2009.

[73] Aiko K Thompson, Ferne R Pomerantz, and Jonathan R Wolpaw. Operant conditioning of a spinal reflex can improve locomotion after spinal cord injury in humans. *Journal of Neuroscience*, 33(6):2365–2375, 2013.

[74] Frank Tong. Primary visual cortex and visual awareness. *Nature Reviews Neuroscience*, 4(3):219–229, 2003.

[75] Vincent Walsh and Alan Cowey. Transcranial magnetic stimulation and cognitive neuroscience. *Nature Reviews Neuroscience*, 1(1):73–80, 2000.

[76] Takeo Watanabe, Yuka Sasaki, Kazuhisa Shibata, and Mitsuo Kawato. Advances in fMRI real-time neurofeedback. *Trends in cognitive sciences*, 2017.

[77] Nikolaus Weiskopf, Klaus Mathiak, Simon W Bock, Frank Scharnowski, Ralf Veit, Wolfgang Grodd, Rainer Goebel, and Niels Birbaumer. Principles of a brain-computer interface (BCI) based on real-time functional magnetic resonance imaging (fMRI). *IEEE transactions on biomedical engineering*, 51(6):966–970, 2004.

[78] Marijke Welvaert and Yves Rosseel. On the definition of signal-to-noise ratio and contrast-to-noise ratio for fmri data. *PloS one*, 8(11):e77089, 2013.

[79] Tobias Wiestler and Jörn Diedrichsen. Skill learning strengthens cortical representations of motor sequences. *Elife*, 2, 2013.

[80] Tobias Wiestler, David J McGonigle, and Jörn Diedrichsen. Integration of sensory and motor representations of single fingers in the human cerebellum. *Journal of neurophysiology*, 105(6):3042–3053, 2011.

[81] Tobias Wiestler, Sheena Waters-Metenier, and Jörn Diedrichsen. Effector-independent motor sequence representations exist in extrinsic and intrinsic reference frames. *Journal of Neuroscience*, 34(14):5054–5064, 2014.

[82] Matthias Witte, Silvia Erika Kober, Manuel Ninaus, Christa Neuper, and Guilherme Wood. Control beliefs can predict the ability to up-regulate sensorimotor rhythm during neurofeedback training. *Frontiers in human neuroscience*, 7, 2013.

[83] Jonathan R Wolpaw. Operant conditioning of primate spinal reflexes: the h-reflex. *Journal of Neurophysiology*, 57(2):443–459, 1987.

[84] J. Xu, N. Ejaz, B. Hertler, M. Branscheidt, M. Widmer, N. Kim, M. Harran, J. C. Cortes, A. V. Faria, P. A. Celnik, T. Kitago, A. Luft, J. W. Krakauer, and J. Diedrichsen. Changes in neural activity patterns during recovery of fine finger control after stroke. In *45th Annual Meeting of Society for Neuroscience (SfN), Chicago*, 2015.

[85] Jing Xu, Naveed Ejaz, Benjamin Hertler, Meret Branscheidt, Mario Widmer, Andreia V Faria, Michelle D Harran, Juan C Cortes, Nathan Kim, Pablo A

Celnik, et al. Separable systems for recovery of finger strength and control after stroke. *Journal of neurophysiology*, 118(2):1151–1163, 2017.

[86] Okito Yamashita, Masa-aki Sato, Taku Yoshioka, Frank Tong, and Yukiyasu Kamitani. Sparse estimation automatically selects voxels relevant for the decoding of fmri activity patterns. *NeuroImage*, 42(4):1414–1429, 2008.

[87] Atsushi Yokoi, Spencer A Arbuckle, and Jörn Diedrichsen. The role of human primary motor cortex in the production of skilled finger sequences. *Journal of Neuroscience*, 38(6):1430–1442, 2018.

[88] Seung-Schik Yoo and Ferenc A Jolesz. Functional mri for neurofeedback: feasibility studyon a hand motor task. *Neuroreport*, 13(11):1377–1381, 2002.

[89] Steven R Zeiler, Robert Hubbard, Ellen M Gibson, Tony Zheng, Kwan Ng, Richard O'Brien, and John W Krakauer. Paradoxical motor recovery from a first stroke after induction of a second stroke: reopening a postischemic sensitive period. *Neurorehabilitation and neural repair*, 30(8):794–800, 2016.

[90] Steven R Zeiler and John W Krakauer. The interaction between training and plasticity in the post-stroke brain. *Current opinion in neurology*, 26(6):609, 2013.

Vita

Ethan Frank Oblak was born in Victoria, Canada. He received the Bachelor of Applied Science in Systems Design Engineering from the University of Waterloo in April, 2013. He began graduate studies in Mechanical Engineering at the University of Texas at Austin in August, 2013.

Email: eoblak@utexas.edu

This dissertation was typeset with LaTeX[†] by the author.

[†] LaTeX is a document preparation system developed by Leslie Lamport as a special version of Donald Knuth's TeX Program.